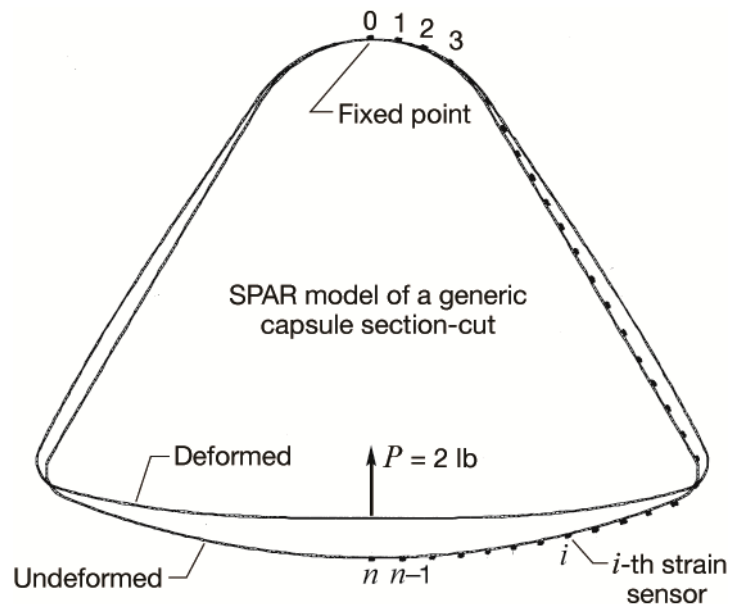


Modified Displacement Transfer Functions for Deformed Shape Predictions of Slender Curved Structures with Varying Curvatures

*William L. Ko and Van Tran Fleischer
Armstrong Flight Research Center, Edwards, California*



PATENT PROTECTION NOTICE

The method for structural shape predictions using distributed surface strains and embodied Ko Displacement Transfer Functions for transforming into structure deformed shapes described in this NASA report is protected under *Method for Real-Time Structure-Shape Sensing*, U.S. Patent No. 7,520,176 issued April 21, 2009. Therefore, those interested in using the method should contact the NASA Innovative Partnership Program Office at NASA Armstrong Flight Research Center, Edwards, California, for more information.

NASA STI Program ... in Profile

Since its founding, NASA has been dedicated to the advancement of aeronautics and space science. The NASA scientific and technical information (STI) program plays a key part in helping NASA maintain this important role.

The NASA STI program operates under the auspices of the Agency Chief Information Officer. It collects, organizes, provides for archiving, and disseminates NASA's STI. The NASA STI program provides access to the NASA Aeronautics and Space Database and its public interface, the NASA Technical Reports Server, thus providing one of the largest collections of aeronautical and space science STI in the world. Results are published in both non-NASA channels and by NASA in the NASA STI Report Series, which includes the following report types:

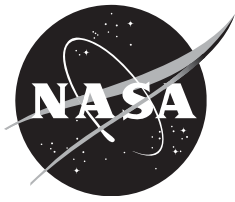
- **TECHNICAL PUBLICATION.** Reports of completed research or a major significant phase of research that present the results of NASA Programs and include extensive data or theoretical analysis. Includes compilations of significant scientific and technical data and information deemed to be of continuing reference value. NASA counter-part of peer-reviewed formal professional papers but has less stringent limitations on manuscript length and extent of graphic presentations.
- **TECHNICAL MEMORANDUM.** Scientific and technical findings that are preliminary or of specialized interest, e.g., quick release reports, working papers, and bibliographies that contain minimal annotation. Does not contain extensive analysis.
- **CONTRACTOR REPORT.** Scientific and technical findings by NASA-sponsored contractors and grantees.
- **CONFERENCE PUBLICATION.** Collected papers from scientific and technical conferences, symposia, seminars, or other meetings sponsored or co-sponsored by NASA.
- **SPECIAL PUBLICATION.** Scientific, technical, or historical information from NASA programs, projects, and missions, often concerned with subjects having substantial public interest.
- **TECHNICAL TRANSLATION.** English-language translations of foreign scientific and technical material pertinent to NASA's mission.

Specialized services also include organizing and publishing research results, distributing specialized research announcements and feeds, providing information desk and personal search support, and enabling data exchange services.

For more information about the NASA STI program, see the following:

- Access the NASA STI program home page at <http://www.sti.nasa.gov>
- E-mail your question to help@sti.nasa.gov
- Fax your question to the NASA STI Information Desk at 443-757-5803
- Phone the NASA STI Information Desk at 443-757-5802
- Write to:
STI Information Desk
NASA Center for AeroSpace Information
7115 Standard Drive
Hanover, MD 21076-1320

NASA/TM—2014–216660



Modified Displacement Transfer Functions for Deformed Shape Predictions of Slender Curved Structures with Varying Curvatures

*William L. Ko and Van Tran Fleischer
Armstrong Flight Research Center, Edwards, California*

National Aeronautics and
Space Administration

*Armstrong Flight Research Center
Edwards, CA 93523-0273*

May 2014

Available from:

NASA Center for AeroSpace Information
7115 Standard Drive
Hanover, MD 21076-1320
443-757-5802

TABLE OF CONTENTS

ABSTRACT	1
NOMENCLATURE.....	1
INTRODUCTION	2
BASICS OF THE DISPLACEMENT TRANSFER FUNCTIONS	3
Curvature Equations.....	4
Shifted Curvature-Strain Equation.....	4
Integrations of the Shifted Curvature-Strain Equation.....	5
1. Discretization	5
2. Basic Assumptions.....	5
3. Slope Equation	6
4. Deflection Equation	6
DISPLACEMENT TRANSFER FUNCTIONS	6
For Cantilever Straight Beams.....	6
For Two-End Supported Straight Beams.....	7
1. Two-End Clamped Beams.....	8
2. Two-End Simply Supported Beams.....	8
3. Calculations of y_i	8
ANALYTICAL SHAPE PREDICTIONS	8
SHAPE PREDICTIONS OF TWO-END SUPPORTED CURVED BEAMS.....	9
Geometry.....	9
Clamped Curved Beams.....	10
1. Deformed Shapes	10
2. Surface Bending Strain Curves.....	10
3. Deflection Curves	10
4. Curvature-Effect Corrections.....	11
5. Values of η	12
Simply Supported Curved Beams	12
1. Deformed Shapes.....	12
2. Surface Bending Strain Curves.....	13
3. Deflection Curves	13
4. Curvature-Effect Corrections.....	13
5. Values of $\{\eta_1, \eta_2\}$	14
SHAPE PREDICTIONS OF GENERIC CAPSULE (GC) OUTER SHELL.....	14
Geometry.....	15
Surface Bending Strain Curve.....	15
Deflection Equation	16
Deflection Curves.....	16
DISCUSSION.....	17
CONCLUDING REMARKS.....	17

FIGURES	19
REFERENCES.....	38

ABSTRACT

To eliminate the need to use finite-element modeling for structure shape predictions, a new method was invented. This method is to use the Displacement Transfer Functions to transform the measured surface strains into deflections for mapping out overall structural deformed shapes. The Displacement Transfer Functions are expressed in terms of rectilinearly distributed surface strains, and contain no material properties. This report is to apply the patented method to the shape predictions of non-symmetrically loaded slender curved structures with different curvatures up to a full circle. Because the measured surface strains are not available, finite-element analysis had to be used to analytically generate the surface strains. Previously formulated straight-beam Displacement Transfer Functions were modified by introducing the curvature-effect correction terms. Through single-point or dual-point collocations with finite-element-generated deflection curves, functional forms of the curvature-effect correction terms were empirically established. The resulting modified Displacement Transfer Functions can then provide quite accurate shape predictions. Also, the uniform straight-beam Displacement Transfer Function was applied to the shape predictions of a section-cut of a generic capsule (GC) outer curved sandwich wall. The resulting GC shape predictions are quite accurate in partial regions where the radius of curvature does not change sharply.

NOMENCLATURE

GC	generic capsule
SPAR	Structural Performance and Resizing finite-element computer program
TPS	Thermal Protection System
c	depth factor of uniform beam, in.
$c(x)$	depth factor of nonuniform beam at x -cross section, in.
c_i	depth factor of nonuniform beam at strain-sensing station x_i , in.
c_0	value of c_i at wing root strain-sensing station x_0 , in.
c_n	value of c_i at wing tip strain-sensing station x_n , in.
ds	small arc length along s , in.
dx	small length along x axis, in.
dy	small length along y axis, in.
$d\theta$	small angle subtended by small arc length ds , rad
E	Young's modulus, lb/in ²
h	beam depth, in
I	moment of inertia, in ⁴
i	= 0,1,2,3,,..., n , strain-sensing station identification number
j	dummy index
l	length of beam, in.
n	index associated with the last span-wise strain-sensing station $x_n(=l)$
$R(x)$	radius of curvature at point x , in.
s	axial coordinate along beam elastic curve, in.
x, y	Cartesian coordinates with origin at beam fixed end (x -axis in beam-axis direction), in.
y	beam deflection normal to x -axis, in.
x_i	x -coordinate (or symbol) of i -th strain-sensing station, in.
x_n	x -coordinate (or symbol) of n -th strain-sensing station, in.
y_i	deflection of cantilever straight beam at strain-sensing station x_i , in.
y_n	deflection of cantilever straight beam at strain-sensing station x_n , in.

y_i^B	deflection of two-end supported straight beam at strain-sensing station x_i , in.
y_p^B	predicted deflection at load application point, p -th strain-sensing station, in.
y_i^C	radial deflection of curved beam at the i -th strain-sensing station calculated from SPAR program, in.
y_p^C	SPAR-generated deflection of curved beam at load application point, p -th strain-sensing station, in.
\hat{y}_i	radial deflection of cantilever curved beam at the i -th strain-sensing station, in.
\hat{y}_i^B	radial deflection of two-end supported curved beam at i -th strain-sensing station, in.
$(y_i)_{GC}$	deflection of GC section-cut at i -th strain-sensing station, in.
Δl	$= l/n$, domain length (distance between any two adjacent strain-sensing stations), in.
$\Delta\phi$	$\equiv \phi_n / n$, curved beam domain angle, rad or deg
ε_i	surface bending strain at i -th strain-sensing station, in/in.
$\varepsilon(x)$	surface bending strain at cross section x , in/in.
η	amplitude of sine correction functions for two-end clamped curved beams, in.
η_1, η_2	amplitudes of sine correction functions for two-end simply supported curved beams, in.
η_{GC}	amplitude of sine correction functions for GC curved beams, in.
η_{GC}	deflection correction factor for GC section-cut, no dimension
θ	slope angle, rad or deg
θ_i	slope angle at i -th strain-sensing station, rad or deg
ϕ_i	angular coordinate (measured from beam fixed end) of the i -th strain-sensing station, deg
ϕ_n	angular coordinate of the n -th (last) strain-sensing station (called curved-beam angle), deg

INTRODUCTION

The deflections of a structure under load can be experimentally measured using position transducers or photogrammetry. However, these methods are impractical for airborne structures. Traditionally, deflections of a loaded structure can be analytically predicted by using finite-element method. Depending on the structure, finite-element modeling can be quite complex and very time consuming. To eliminate the need for tedious finite-element modeling, a new innovative method called *Method for Real-Time Structure Shape Sensing* (U.S. Patent Number 7,520,176) was invented. This patented method is to use measured surface strains for input into the Displacement Transfer Functions (refs. 1–9) to calculate deflections so that one can map out the overall structural deformed shapes for visual displays. Keep in mind that without using the Displacement Transfer Functions, the surface strain sensors can only sense the in-plane strains, but not the out-of-plane deflections, nor the cross-sectional rotations of the structure. This innovative structural shape prediction technology is very attractive for application to in-flight deformed shape monitoring of flexible wings and tails, such as those often employed on unmanned flight vehicles by the ground-based pilot for maintaining safe flights. In addition, the real-time wing shape monitored could then be input to the aircraft control system for aero-elastic wing shape control.

In the formulation of the earlier Displacement Transfer Functions (refs. 1–9), the embedded beam (defined as the depth-wise cross section of a structure along the strain-sensing line) was first discretized into multiple small domains of equal length, so that within each small domain, the beam depth and surface bending strain can be assumed to vary linearly. This discretization approach enabled piecewise integrations

of the beam curvature equation in closed forms to yield beam slope and deflection equations in recursive forms. Those recursive slope and deflection equations were then combined into a single deflection equation in dual summation form called the Displacement Transfer Function, written in terms of beam geometrical parameters and surface strains along the strain-sensing line. By inputting the surface strain data, the Displacement Transfer Function can convert the surface strains into the embedded beam slopes and deflections along the strain-sensing line. By using multiple strain-sensing lines, one can then graphically map out the overall structural deformed shapes (under combined bending and torsion) for visual display.

The surface strains and the Displacement Transfer Functions could also be used in a new operational load sensing technology, called *Improved Process for Using Surface Strain Measurements to Obtain Operational Loads for Complex Structures* (U.S. Patent No. 7,715,994) (ref. 10), for the estimations of in-flight wing operational loads (bending moments, shear loads, and torques).

The Displacement Transfer Functions (refs. 1–9) were originally developed for the deformed shape predictions of straight slender structures, and their shape prediction accuracies were successfully validated by using finite-element analyses of different sample structures such as cantilever tubular beams (uniform, tapered, slightly tapered, and step-wisely tapered), two-end supported tapered tubular beams, flat panels, and tapered wing boxes (un-swept and swept). Also, experimentally, the shape prediction accuracies of the Displacement Transfer Functions (refs. 1–9) were validated by deflections measured from photogrammetry in the Global Observer (175 ft wingspan) ground loads tests (ref. 11).

For the shape predictions of curved structures, curvature effect will show up. Without going through standard mathematical formulations, previously formulated straight-beam Displacement Transfer Functions (refs. 1–9) can be modified by introducing curvature-effect correction terms to obtain the modified Displacement Transfer Functions for the curved structures.

For symmetrically loaded curved beams with different curvatures up to a full circle (ref. 12), the functional forms of the curvature-effect correction terms were empirically established through single-point collocations using finite-element generated deflection curves. The resulting empirically established curved-beam Displacement Transfer Functions can then provide quite accurate shape predictions.

The present report deals with the shape predictions of more general cases of non-symmetrically loaded slender curved structures with varying curvatures up to a full circle. Similar to the symmetrical loading cases (ref. 12); the straight-beam Displacement Transfer Functions (refs. 1–9) were modified by introducing the curvature-effect correction terms. Because the measured surface strain data are not available, finite-element analysis was used to analytically generate the input surface strains and deflections (to be used as reference yardsticks). The functional forms of the curvature-effect correction terms were then empirically established through either single point or dual-point collocations with the finite-element-generated deflection curves. The results show that the modified Displacement Transfer Functions can provide quite accurate shape predictions of non-symmetrically loaded curved beams up to a full circle.

Also, the shape prediction analysis was conducted on the curved beam embedded in a section-cut of a generic capsule (GC) outer shell wall. The resulting shape predictions are fairly accurate except for the sharply curved regions.

BASICS OF THE DISPLACEMENT TRANSFER FUNCTIONS

The term, beam, used in the present report implies the embedded beam, which is defined as the depth-wise cross section of structure along the surface strain-sensing line (refs. 1–9). The Displacement Transfer Functions formulated for the straight embedded beams is briefly described below. The key assumptions made in the mathematical formulation of the theory are also discussed.

Curvature Equations

Figure 1 shows a deformed nonuniform embedded beam with varying depth factor, $c(x)$. In a small beam segment subtended by $d\theta$, the small undeformed curve length, $AB(= ds)$, is on the beam neutral axis, and the deformed curve length, $A'B'\{= AB[1 + \varepsilon(x)] = ds[1 + \varepsilon(x)]\}$, lies on the beam lower surface under bending strain, $\varepsilon(x)$. From the two similar slender sectors, $O'AB$ and $O'A'B'$, the local radius of curvature, $R(x)$, of the beam elastic curve can be related to the lower surface bending strain, $\varepsilon(x)$, through the beam depth factor, $c(x)$, as equation (1):

$$\frac{O'A'}{O'A} = 1 + \frac{c(x)}{R(x)} = \frac{A'B'}{AB} = 1 + \varepsilon(x) \quad (1)$$

which yields the curvature-strain relationship as equation (2):

$$\frac{1}{R(x)} = \frac{\varepsilon(x)}{c(x)} \quad (2)$$

Equation (2) geometrically relates the local curvature, $1/R(x)$, of the deformed embedded beam elastic curve to the associated surface bending strain, $\varepsilon(x)$, and the embedded beam depth factor, $c(x)$.

The physical (Lagrangian) curvature equation can be written as equation (3) (derivations in ref. 8):

$$\frac{1}{R(x)} = \frac{d^2y/dx^2}{\sqrt{1 - (dy/dx)^2}} \quad (3)$$

in which x is the undeformed axial coordinate, and y is the out-of-plane deflection.

Combining equations (2) and (3), one obtains the physical (Lagrangian) curvature-strain relationship as equation (4):

$$\frac{d^2y/dx^2}{\sqrt{1 - (dy/dx)^2}} = \frac{\varepsilon(x)}{c(x)} \quad (4)$$

Shifted Curvature-Strain Equation

In the beam bending deformations, the axial displacement is very small. If axial displacement is set to zero, the term, $(dy/dx)^2$, in equation (4) will also become zero (ref. 7). Then equation (4) becomes:

$$\frac{d^2y}{dx^2} = \frac{\varepsilon(x)}{c(x)} \quad (5)$$

Equation (5) is called the Shifted curvature-strain equation for nonuniform embedded beams, which is purely a geometrical relationship containing no material properties. Because equation (5) is referred to the undeformed x -coordinate (Lagrangian formulation), the term, d^2y/dx^2 , in equation (5) is not the simplified

form of the classical mathematical curvature equation, $\frac{1}{R(x)} = \frac{d^2y/dx^2}{[1+(dy/dx)^2]^{3/2}}$, which is in reference to the deformed x -coordinate (Eulerian formulation) when applied to deformed embedded beams (ref. 7).

Integrations of the Shifted Curvature-Strain Equation

For a given beam geometry, the functional form of the depth factor, $c(x)$, is known. However the distribution of the surface strain, $\varepsilon(x)$, in general varies nonlinearly along the nonuniform beam and cannot be described with a simple mathematical function. Therefore, the piecewise integration method can be used. Namely, by piecewise representations of $\{c(x), \varepsilon(x)\}$, the Shifted curvature-strain equation (5) can be integrated for each domain once to yield beam slopes, and the second integration can yield beam deflections, both of which are needed for the structure deformed shape predictions. This piecewise approach was used in the formulations of the earlier Displacement Transfer Functions for the embedded straight beams (refs. 1–7). The following sections briefly describe the piecewise integration method.

1. Discretization

To carry out the piecewise integrations of equation (5) in closed form, the nonuniform embedded beam of length, l , (fig. 2) was first discretized into n small domains of equal length, $\Delta l (= l/n)$, (fig. 2). The i -th ($i = 0, 1, 2, 3, \dots, n$) strain-sensing stations are to be located on the lower surface of the domain junctures, $x = x_i$ ($i = 0, 1, 2, 3, \dots, n$), (called strain-sensing stations x_i). Note from figure 2 that the first and the last strain-sensing stations, $\{x_0, x_n\}$, are located respectively at the fixed end, ($x = x_0 = 0$), and at the free end, ($x = x_n = l$). Within each small domain, $x_{i-1} \leq x \leq x_i$, between the two adjacent strain-sensing stations, $\{x_{i-1}, x_i\}$, the following piecewise linear assumptions can be made with sufficient accuracies for slowly changing functions.

2. Basic Assumptions

The two basic assumptions needed for deriving the Displacement Transfer Functions are given below:

Within a small domain, $x_{i-1} \leq x \leq x_i$, between the two adjacent strain-sensing stations, $\{x_{i-1}, x_i\}$; the depth factor, $c(x)$; and the lower surface bending strain, $\varepsilon(x)$, can be represented with linear functions of $(x - x_{i-1})$ as:

$$c(x) = c_{i-1} - (c_{i-1} - c_i) \frac{x - x_{i-1}}{\Delta l} \quad ; \quad x_{i-1} \leq x \leq x_i \quad (6)$$

$$\varepsilon(x) = \varepsilon_{i-1} - (\varepsilon_{i-1} - \varepsilon_i) \frac{x - x_{i-1}}{\Delta l} \quad ; \quad x_{i-1} \leq x \leq x_i \quad (7)$$

In equation (6), $\{c_{i-1}, c_i\}$ are respectively the values of $c(x)$ at the strain-sensing stations, $\{x_{i-1}, x_i\}$. Similarly, in equation (7), $\{\varepsilon_{i-1}, \varepsilon_i\}$ are respectively the values of $\varepsilon(x)$ at the strain-sensing stations, $\{x_{i-1}, x_i\}$.

If $\{c(x), \varepsilon(x)\}$ are strong nonlinear functions of x , the domain length, Δl , should be reduced so that the piecewise linear assumptions [eqs. (6), (7)] could still be good approximations.

3. Slope Equation

The slope, $\tan \theta(x)$, of the nonuniform beam at axial location, x , within the domain, $x_{i-1} \leq x \leq x_i$ (fig. 2), can be obtained by piecewise integration of equation (5), and enforcing the continuity of slope at the inboard strain-sensing station, x_{i-1} , as equation (8):

$$\tan \theta(x) = \underbrace{\int_{x_{i-1}}^x \frac{d^2 y}{dx^2} dx}_{\text{Piecewise integration of curvature equation (5)}} + \underbrace{\tan \theta_{i-1}}_{\text{Slope at } x_{i-1}} = \underbrace{\int_{x_{i-1}}^x \frac{\varepsilon(x)}{c(x)} dx}_{\text{Slope increment above } \tan \theta_{i-1}} + \underbrace{\tan \theta_{i-1}}_{\text{Slope at } x_{i-1}} ; \quad (x_{i-1} \leq x \leq x_i) \quad (8)$$

in which $\tan \theta_{i-1}$ is the slope at the inboard strain-sensing station, x_{i-1} .

4. Deflection Equation

The deflection, $y(x)$, of the nonuniform beam within the domain, $x_{i-1} \leq x \leq x_i$ (fig. 2), can be obtained by piecewise integration of the slope equation (8) and enforcing the continuity of deflection at the inboard adjacent strain-sensing station, x_{i-1} , as:

$$y(x) = \underbrace{\int_{x_{i-1}}^x \tan \theta(x) dx}_{\text{Piecewise integration of slope equation (8)}} + \underbrace{y_{i-1}}_{\text{Deflection at } x_{i-1}} = \underbrace{\int_{x_{i-1}}^x \int_{x_{i-1}}^x \frac{\varepsilon(x)}{c(x)} dx dx}_{\text{Deflection increment above } y_{i-1}} + \underbrace{\int_{x_{i-1}}^x \tan \theta_{i-1} dx}_{\text{Deflection at } x \text{ due to } \tan \theta_{i-1}} + \underbrace{y_{i-1}}_{\text{Deflection at } x_{i-1}} \quad (9)$$

$(x_{i-1} \leq x \leq x_i)$

in which y_{i-1} is the deflection at the inboard strain-sensing station, x_{i-1} .

In light of the linearity assumptions of $\{c(x), \varepsilon(x)\}$ given respectively by equations (6) and (7), equations (8) and (9) can now be integrated once and twice respectively to yield the recursive forms of slope and deflection equations for each domain. The recursive slope and deflection equations were then combined into a single deflection equation in dual summation form, called the Displacement Transfer Function for the embedded beam along the strain-sensing line (refs. 1–9).

DISPLACEMENT TRANSFER FUNCTIONS

The Displacement Transfer Functions formulated earlier for straight cantilever embedded beams and for straight two-point supported embedded beams are listed below.

For Cantilever Straight Beams

Typical Displacement Transfer Functions previously formulated for nonuniform, slightly nonuniform, and uniform cantilever straight embedded beams have the following mathematical forms (refs. 1–9).

1. For nonuniform cantilever beams, $(c_i \neq c_{i-1})$ (see derivation in Appendix A of ref. 2):

$$y_i = (\Delta l)^2 \sum_{j=1}^i \left\{ [2(i-j)+1] \frac{\varepsilon_{j-1} - \varepsilon_j}{2(c_{j-1} - c_j)} - \frac{\varepsilon_{j-1}c_j - \varepsilon_jc_{j-1}}{(c_{j-1} - c_j)^3} \left[c_j \log \frac{c_j}{c_{j-1}} + (c_{j-1} - c_j) \right] \right\} \\ + (\Delta l)^2 \sum_{j=1}^{i-1} (i-j) \left[\frac{\varepsilon_{j-1}c_j - \varepsilon_jc_{j-1}}{(c_{j-1} - c_j)^2} \log \frac{c_j}{c_{j-1}} \right] + \underbrace{y_0 + (i)\Delta l \tan \theta_0}_{=0 \text{ for cantilever beam}} \quad (i=1,2,3,\dots,n) \quad (10)$$

Equation (10) cannot be used directly for the uniform beams, ($c_i = c_{i-1} = c$), because the logarithmic terms, $\log_e(c_j/c_{j-1})$, and the factor, $(c_{j-1} - c_j)$, appearing in the denominators will go to zero, causing mathematical indeterminacy (0/0).

2. For slightly nonuniform cantilever beams ($c_i/c_{i-1} \rightarrow 1$) (see derivation in Appendix C of ref. 2):

$$y_i = \frac{(\Delta l)^2}{6} \sum_{j=1}^i \frac{1}{c_{i-j}} \left\{ \left[3(2j-1) - (3j-2) \frac{c_{i-j+1}}{c_{i-j}} \right] \varepsilon_{i-j} + (3j-2) \varepsilon_{i-j+1} \right\} + \underbrace{y_0 + (i)\Delta l \tan \theta_0}_{=0 \text{ for cantilever beam}} \quad (i=1,2,3, \dots, n) \quad (11)$$

Equation (11) was obtained from equation (8) by expanding the logarithmic terms in the neighborhood of $c_i/c_{i-1} \approx 1$ (see derivations in Appendix C of ref. 2). Equation (11) may also be used for uniform beams, ($c_i = c_{i-1} = c$), without encountering limit case mathematical problem like equation (10).

3. For uniform straight cantilever beams ($c_i = c_{i-1} = c$) (see derivation in Appendix D of ref. 2):

$$y_i = \frac{(\Delta l)^2}{6c} \left[(3i-1)\varepsilon_0 + 6 \sum_{j=1}^{i-1} (i-j)\varepsilon_j + \varepsilon_i \right] + \underbrace{y_0 + (i)\Delta l \tan \theta_0}_{=0 \text{ for cantilever beam}} \quad ; \quad (i=1,2,3, \dots, n) \quad (12)$$

Equation (12) was obtained by grouping terms after setting $c_i = c_{i-1} = c$ in equation (11).

In each of the Displacement Transfer Functions [equations (10) to (12)], the deflection, y_i , at the strain-sensing station, x_i , is expressed in terms of the inboard beam depth factors, $(c_0, c_1, c_2, \dots, c_i)$, and the associated inboard strains, $(\varepsilon_0, \varepsilon_1, \varepsilon_2, \dots, \varepsilon_i)$, including the values of $\{c_i, \varepsilon_i\}$ at the strain-sensing station, x_i , where deflection, y_i , is calculated.

Equations (10) to (12) are purely geometrical relationships, containing only the beam geometry and surface strains, and no material property is involved. In fact, the material property will affect the values of the surface strains. Thus, in using equations (10) to (12) for shape predictions of complex structures (for example, aircraft wings); there is no need to know the material property, nor the geometries of the complex internal structures.

For Two-End Supported Straight Beams

The Displacement Transfer Functions [equations (10) to (12)] formulated for cantilever straight beams were extended for the two-end supported straight beams under different support conditions (ref. 11). The deflections, y_i^B , of the two-end supported beams can then be expressed as follows:

1. Two-End Clamped Beams

By enforcing zero slope and zero deflection at the left support, and enforcing zero deflection at the right support, the deflection equation for the two-end clamped beams was formulated as equation (13) (ref. 11):

$$y_i^B = y_i - \underbrace{\left(\frac{i}{n}\right)^2}_{\substack{\text{To enforce} \\ y_n^B = 0 \text{ at right} \\ \text{support } (i=n)}} y_n \quad ; \quad (i=1,2,3, \dots, n) \quad (13)$$

In equation (13) y_n is the small deflection error at the clamped right end because of using equation (10), (11), or (12) for cantilever beams. Therefore, $(i/n)^2 y_n$ term is used to enforce $y_n^B = 0$ at the clamped right end, ($i = n$), and also minimize the correction disturbance of zero slope at the clamped left end. When the surface strains of the two-end clamped case are used, the generated deflection curve gives zero slope at the clamped right end. As will be seen shortly, for the straight beam, the error, y_n , is extremely small, however, as the beam curvature increases, the error, y_n , will also increase.

2. Two-End Simply Supported Beams

By enforcing zero displacements at the left and right ends, the deflection equation the two-end simply supported beams was established as equation (14) (see graphical illustration in fig. 4 of ref. 2):

$$y_i^B = y_i - \underbrace{\frac{i}{n}}_{\substack{\text{To enforce} \\ y_n^B = 0 \text{ at right} \\ \text{support } (i=n)}} y_n \quad ; \quad (i=1,2,3, \dots, n) \quad (14)$$

In equation (14) y_n is the maximum deflection of the cantilever beam at the right free end. Therefore, the term, $(i/n)y_n$, is needed to bring the displacement to zero ($y_n^B = 0$) at the right end for the simply supported beams.

3. Calculations of y_i

In equations (13) and (14), y_i is the deflection of a cantilever straight beam and can be calculated from equation (10), (11), or (12) depending on the type of beam. In the present report, all the curved beams considered have uniform depths. Therefore, only equation (12) (for uniform cantilever straight beams) was used in equations (13) and (14) to empirically establish the modified Displacement Transfer Functions for non-symmetrically loaded slender curved beams under different support conditions.

ANALYTICAL SHAPE PREDICTIONS

The shape prediction study presented in this report is called analytical shape prediction study. Because the experimentally measured surface strains, $\varepsilon_i (i = 0,1,2,3,\dots,n)$, were not available, the needed surface strains had to be analytically generated. The Structural Performance And Resizing (SPAR) finite-element computer program (ref. 13) was used to generate the surface strains, ε_i , by converting SPAR element (or nodal) stresses into element (or nodal) strains through stress-strain relationship. As mentioned earlier, if the measured surface strain data are available, finite-element analysis is not needed.

The SPAR-generated surface strains, ϵ_s , were then input to the straight-beam Displacement Transfer Functions [eqs. (13) or (14)] to calculate the theoretical deflection curves. By comparing the theoretical deflection curves with the corresponding SPAR-generated deflection curves (reference yardsticks), the functional forms of the curvature-effect correction terms for establishing the modified Displacement Transfer Functions can be determined empirically.

SHAPE PREDICTIONS OF TWO-END SUPPORTED CURVED BEAMS

In establishing the functional forms of the curvature-effect correction terms for non-symmetrically loaded two-end supported curved beams, the whole range of curved-beam angle, ($0^\circ \leq \phi_n \leq 360^\circ$), was considered.

Geometry

For establishing the modified Displacement Transfer Functions for non-symmetrically loaded curved beams, the two-end supported curved beams with different curvatures were used for the shape prediction analyses. Table 1 lists the dimensions of the two-end supported curved beams analyzed.

Table 1. Dimensions of two-end supported curved beams; width = 1 in.; $c = 0.25$ in.

l , in.	ϕ_n , deg	R , in.	h , in.	c , in.	R/c
200	0 (Straight)	∞	0.50	0.25	∞
200	45 (1/8 circle)	254.65	0.50	0.25	1019
200	90 (1/4 circle)	127.32	0.50	0.25	509
200	135 (3/8 circle)	84.88	0.50	0.25	340
200	180 (1/2 circle)	63.66	0.50	0.25	255
200	225 (5/8 circle)	50.93	0.50	0.25	204
200	270 (3/4 circle)	42.44	0.50	0.25	170
200	315 (7/8 circle)	36.38	0.50	0.25	146
200	360 (Full circle)	31.83	0.50	0.25	127

All of the two-end supported curved beams analyzed have a unit width, an identical curved length of $l = 200$ in., and a constant depth factor of $c = 0.25$ in. (half depth). To maintain the same curved beam length, the radius of curvature R was changed with respect to the change of the curved beam angle, ϕ_n . For the range of radius-of-curvature factor of R/c listed in table 1, the neutral axis offset is practically zero (fig. 2 of ref. 11), and therefore, it was ignored in the current shape prediction analysis.

Figure 3 shows a typical two-end supported curved beam under two types of support conditions: 1) both ends clamped (clamped curved beam), and 2) both ends simply supported (simply supported curved beam). As shown in figure 3, there are $n+1$ ($n = 32$) equally spaced strain-sensing stations, identified with i ($= 0, 1, 2, 3, \dots, n$), along the curved beam outer surface. Inner surface strains are not needed because the location of the neutral axis is known (depth factor c is known).

Each of the two-end supported curved beams is non-symmetrically loaded with an inward radial load of $P = 2$ lb at the curved beam three-quarter point, $\phi_i = (3/4)\phi_n$, which is located at the strain-sensing station $i = 24$ (fig. 3).

Clamped Curved Beams

The following sections discuss the deformed shapes, surface bending strains, and deflections of the two-end clamped curved beams. Also, the formulations of the modified Displacement Transfer Function for the clamped curved beams are discussed.

1. Deformed Shapes

Figure 4 shows the undeformed and deformed shapes of the asymmetrically loaded clamped curved beams models generated by the SPAR program. For the straight clamped beam, ($\phi_n = 0^\circ$, fig. 4), the maximum deflection point did not coincide with the loading point, but is located slightly on the left hand side of the loading point. In the range of curved beam angles, ($45^\circ \leq \phi_n \leq 180^\circ$), the right hand loading region caved in, but the left hand region bulged out. For a deeper curved beam in the range of ($225^\circ \leq \phi_n \leq 360^\circ$), the load did not induce observable cave-in deformation on the beam right hand side; however, the left hand side of the beam bulge out like the shallow curved beam cases. Thus, the clamped curved beams deformed into distorted sine wave shapes. This observation indicates that for the clamped curved beam cases, two sine functions with same amplitude can be excellent curvature-effect correction functions as shown in the subsequent sections.

2. Surface Bending Strain Curves

As mentioned earlier, the surface bending strains, $\varepsilon_i (i = 0, 1, 2, 3, \dots, n)$, needed for input to the deflection equations for shape predictions were analytically generated from the SPAR program by converting element (or nodal) stresses into associated element (or nodal) strains through stress-strain relationship. Figure 5 shows the SPAR-generated surface bending strain curves for the whole range of curved beam angles, ($0^\circ \leq \phi_n \leq 360^\circ$), including the limit case of straight beam, ($\phi_n = 0^\circ$). For the straight beam (fig. 5), the strain curve consists of two inclined straight lines of different slopes forming a tilted V-shape. For the curved beams, ($\phi_n > 0^\circ$), all the strain curves are flying-bird-wing shaped, and stay quite close near the load application point, but gradually diverged toward both clamped supports.

3. Deflection Curves

The SPAR-generated surface bending strain data (fig. 5) were used as inputs for the calculations of deflection curves. Figures 6(a)–6(i) show the deflection curves calculated from the SPAR program and also from the deflection equation (13) for the whole range of the curved beam angles, ($0^\circ \leq \phi_n \leq 360^\circ$). For the straight clamped beam, [$\phi_n = 0^\circ$, fig. 6(a)], equation (13) provides excellent shape prediction. Even for the $\phi_n = 45^\circ$ curved beam case, equation (13) also gives nice shape prediction. As the curved beam angle, ϕ_n , reached $\phi_n = 90^\circ$ [fig. 6(c)] and continued to increase [figs. 6(d)–6(i)], the shape prediction errors of using the straight-beam deflection equation (13) gradually magnified and reached a maximum error at $\phi_n = 360^\circ$ (circular ring) [fig. 6(i)]. Figures 6(a)–6(i) show that for each curved beam case, the difference between the deflection curves based on SPAR and equation (13) grows from zero at the left support, reaching a maximum at the loading point, and then gradually decreased to zero at the right support. This observation provides the idea that sinusoidal functions are good candidates for the curvature-effect correction functions. The following section discusses the method for establishing the curvature-effect correction terms for the non-symmetrically loaded clamped curved beams.

4. Curvature-Effect Corrections

As shown in figure 6, deflection equation (13) for the clamped straight beam, ($\phi_n = 0^\circ$), could provide quite accurate shape predictions up to $\phi_n = 45^\circ$ curved beams. However, for deeper curved beams, curvature-effect correction terms must be introduced for better shape predictions of curved beams. Note from figures 6(a)–6(i) that for each curved beam angle, ϕ_n , if the loading point of the deflection curve based on equation (13) is moved upward to fit the corresponding point on the SPAR deflection curve (called single point collocation), then the entire deflection curve based on equation (13) will converge toward the associated SPAR deflection curve. This observation suggests that sine functions with proper scaling factors could be the best mathematical forms for the curvature-correction terms.

At the loading point, $i = 24$, of each curved beam case, the difference between the deflection, y_p^B , calculated from equation (13), and the SPAR-generated deflection, y_p^C , can be written as equation (15):

$$\eta \equiv y_p^C - y_p^B \quad (15)$$

in which η (deflection differential) is called the amplitude of the sine correction functions (described below) with dimensions measured in inches.

Through single-point collocations at the load applied point, $i = 24$, two types of sine correction functions were established for the left and right hand sides of the loading point because of non-symmetrical loading. For the symmetrical loading case, only one type of sine correction function is needed (ref. 11). The two modified deflection equations formulated for the whole range of the clamped curved beam, ($0^\circ \leq \phi_n \leq 360^\circ$), un-symmetrically loaded at strain-sensing station, $i = 24$, were established as follows:

For the region on the left-hand side of the loading point, ($0 \leq i \leq 24$):

$$\hat{y}_i^B = y_i - \left(\frac{i}{n}\right)^2 y_n + \eta \sin^4\left(\frac{2}{3}\frac{i}{n}\pi\right) \quad ; \quad (0 \leq i \leq 24) \quad (16a)$$

For the region on the right-hand side of the loading point, ($24 \leq i \leq n$):

$$\hat{y}_i^B = y_i - \left(\frac{i}{n}\right)^2 y_n - \eta \sin\left(2\frac{i}{n}\pi\right) \quad ; \quad (24 \leq i \leq n) \quad (16b)$$

The deflection curves calculated from the modified deflection equations (16) are plotted also in figures 6(a)–6(i) with different values of η indicated for different curvature cases. Note that for the $\phi_n = 45^\circ$ curved beam case [fig. 6(b)], because of negligible value of η , equation (13) for the clamped straight beam gives excellent shape predictions. Therefore, for the shape predictions of any curved beam cases with ϕ_n in the range of ($0^\circ \leq \phi_n \leq 45^\circ$), the straight beam equation (13) can be used.

In the range of ($90^\circ \leq \phi_n \leq 180^\circ$), with only a single point collocation, the deflection curves calculated from equations (16) matched nicely with the corresponding SPAR-deflection curves. At larger curved beam angles, ($225^\circ \leq \phi_n \leq 360^\circ$), the deflection curves calculated from equations (16) deviated slightly from the associated SPAR deflection curves especially in the beam left regions.

5. Values of η

The values of η calculated from equations (16) for single point collocations at the loading point, $i = 24$ for all the clamped curved beams are listed in table 2.

Table 2. Amplitudes, η , of the sine correction function for asymmetrically loaded clamped curved beams; $P = 2$ lb. at $i = 24$; $n = 32$.

ϕ_n , deg	η , in. (Collocation)	η , in. $= (\phi_n/360)^3 \times 1$ in.
0	-----	0.000000
45	0.005706	0.001953
90	0.030645	0.015625
135	0.074517	0.052734
180	0.149139	0.125000
225	0.265637	0.244141
270	0.446214	0.421875
315	0.709179	0.669922
360	1.049224	1.000000

Note from table 2 that for the whole range of curved beam angles, ($0^\circ \leq \phi_n \leq 360^\circ$), the values of η determined from single point collocations can be roughly approximated by a simple function in ϕ_n of the form:

$$\eta \approx \left(\frac{\phi_n}{360} \right)^3 \quad (17)$$

Figure 7 shows the plots of the two types of η (table 2) as functions of the curved beam angle, ϕ_n . The two η curves are quite close. Without collocation processes, the values of η calculated from equation (17) can be used for fairly accurate shape predictions for the non-symmetrically loaded clamped curved beams. The η -curves of figure 7 may be used to obtain other η values for the curved beam angle cases not analyzed, thereby eliminating the single point collocation processes.

Simply Supported Curved Beams

The following sections discuss deformed shapes, surface bending strains, and deflections of the simply supported curved beams.

1. Deformed Shapes

Figure 8 shows undeformed and deformed shapes of the non-symmetrically loaded simply supported curved beam models generated by the SPAR program. For the straight simply supported beam, ($\phi_n = 0^\circ$, fig. 8), the maximum deflection point did not coincide with the loading point, but is located slightly on the left-hand side of the loading point. In the range of curved beam angles, ($45^\circ \leq \phi_n \leq 135^\circ$), the right-hand loading region caved in, but the left-hand region bulged out. For the deeper curved beams in the range of ($180^\circ \leq \phi_n \leq 315^\circ$), the load did not induce observable cave-in deformation on the beam right-hand side; however, the left-hand side of the beam bulged out like the shallow curved beam cases. The case

for $\phi_n = 360^\circ$ is not shown because the two simply supported points are coincidental and offer no resisting moment under non-symmetrical loading, causing indeterminate deflections. Figure 8 shows that the simply supported curved beams deformed into slightly distorted sine wave shapes. This observation indicates that for the simply supported curved beam cases, one-cycle sine function with different amplitudes can be an excellent curvature-effect correction function as shown in the subsequent sections.

2. Surface Bending Strain Curves

As mentioned earlier, the surface bending strains, $\varepsilon_i (i = 0, 1, 2, 3, \dots, n)$, needed for input to deflection equations for shape predictions were analytically generated from the SPAR program by converting element (or nodal) stresses into associated element (or nodal) strains through stress-strain relationship.

Figure 9 shows the SPAR-generated surface bending strain curves for the whole range of curved beam angles, ($0^\circ \leq \phi_n \leq 315^\circ$), including the limit case of the straight beam, ($\phi_n = 0^\circ$). For the straight beam, the strain curve consists of two inclined straight lines (with different slopes) forming a non-symmetrical V-shape. For the curved beams, ($\phi_n > 0^\circ$), all the strain curves exhibit distorted sine waves with a sharp bend at the loading point. The amplitudes (plus and minus) gradually increased as the curvature increased (fig. 9).

3. Deflection Curves

As shown in figures 10(a)–10(h), the deflection equation (14) for the simply supported straight beam, ($\phi_n = 0^\circ$), provides excellent shape predictions for curved beams up to $\phi_n = 45^\circ$. However, for deeper curved beams, ($\phi_n \geq 90^\circ$), the curvature-effect correction terms are needed for better curved-beam shape predictions. Note that each deflection curve formed one cycle of a slightly distorted sine wave with an inflection point located almost at the beam midpoint. Based on this graphical observation [figs. 10(a)–10(h)], sine functions with proper scaling factors were found to be the best mathematical functional forms for the curvature-effect correction terms. Because of non-symmetrical loading, two types of sine correction functions are needed for the left-half and right-half regions of the curved beams. For the symmetrical loading case, only one type of sine correction function was needed (ref. 12). The following section discusses the method for establishing the curvature-effect correction terms for the non-symmetrically loaded simply supported curved beams

4. Curvature-Effect Corrections

Through dual-point collocations at $i = 8$ and $i = 24$ (loading point) in view of the SPAR-generated deflection curves, the curvature-effect correction terms were established for the simply supported curved beams non-symmetrically loaded at the three-quarter point strain-sensing station, $i = 24$. The resulting modified Displacement Transfer Function for the whole range of curved beam angle, ($0^\circ \leq \phi_n \leq 315^\circ$), are shown below.

$$\hat{y}_i^B = y_i - \frac{i}{n} y_n - \eta \sin\left(2 \frac{i}{n} \pi\right) \quad (18)$$

In equation (18), η is the amplitude of the sine correction function; $\eta = \eta_1$ for the left-half Region, ($0 \leq i \leq n/2$), and $\eta = \eta_2$ for the right-half region, ($n/2 \leq i \leq n$). The values of $\{\eta_1, \eta_2\}$ determined through dual-point collocations with the SPAR-generated deflection curves discussed above.

Figures 10(b)–10(h) also show the deflection curves calculated from the modified deflection equation (18) with different values of $\{\eta_1, \eta_2\}$ indicated in each curvature case.

For the $\phi_n = 45^\circ$ curved beam case [fig. 10(b)], the deflection equation (14) for the simply supported straight beam gives excellent shape predictions because of the negligible values of $\{\eta_1, \eta_2\}$. Therefore, for the shape predictions of any curved beams with ϕ_n in the range of $(0^\circ \leq \phi_n \leq 45^\circ)$, the straight beam deflection equation (14) is accurate enough.

In the range of $90^\circ \leq \phi_n \leq 315^\circ$, with dual-point collocations, the deflection curves calculated from equation (18) match nicely with the corresponding SPAR-generated deflection curves.

5. Values of $\{\eta_1, \eta_2\}$

The values of $\{\eta_1, \eta_2\}$ determined from dual-point collocations at $i = 8$ (for η_1) and at the loading point $i = 24$ (for η_2) for all the simply supported curved beams are listed in table 3.

Table 3. Amplitudes, $\{\eta_1, \eta_2\}$, of sine correction functions for non-symmetrically loaded simply supported curved beams.

ϕ_n , deg	η_1 , in.	η_2 , in.	$(\eta_1 + \eta_2)/2$, in.
0	-----	-----	-----
45	0.009527	-0.000056*	0.004792
90	0.040853	0.033365	0.037109
135	0.114164	0.096584	0.105002
180	0.266372	0.238865	0.252619
225	0.623126	0.584682	0.603904
270	1.725869	1.665992	1.695931
315	8.117479	8.011471	9.064475
360	(No resisting moments at two coincidental simply supported points under non-symmetrical loading)		

* Negative scaling factor implies slight over prediction.

Because the values of $\{\eta_1, \eta_2\}$ are quite close, the averaged values, $\eta = (\eta_1 + \eta_2)/2$, are also listed in table 3. The averaged values of $(\eta_1 + \eta_2)/2$ provide reasonably accurate shape predictions for the simply supported curved beams; therefore, equation (18) can be written as a single equation.

Figure 11 shows the plots of $\{\eta_1, \eta_2\}$ (table 3) as functions of the curved beam angle, ϕ_n . The two curves are quite close, and using the averaged values, $(\eta_1 + \eta_2)/2$, can provide fairly accurate shape predictions for the non-symmetrically loaded simply supported curved beams. The $\{\eta_1, \eta_2\}$ -curves of figure 11 can be used to obtain other $\{\eta_1, \eta_2\}$ values associated with other curved beam angle cases not analyzed, thereby eliminating the need to resort to dual-point collocation processes for these cases.

SHAPE PREDICTIONS OF GENERIC CAPSULE (GC) OUTER SHELL

The detailed descriptions of the GC structures for lunar return reentry thermal analysis are presented in reference 14. The following sections show the geometry and the portion of the GC shell analyzed.

Geometry

Figure 12 shows a geometrical shape of the GC outer shell, which is the union of a windward shallow spherical shell, shoulder toroidal shell, leeward cone shell, and apex deep spherical shell. The outer mold-line shape of the GC is practically a modified and scaled up version of an earlier Apollo capsule shape. The fore-body (windward) outer surface is a shallow spherical cap with a 196.85-in. diameter (154.00-in. diameter for the Apollo case) and 246.00-in. radius of curvature (184.8-in. radius of curvature for the Apollo case). The aft-body is a circular cone with side-wall angle of 30.25° (33° for the Apollo capsule) measured from the axis of symmetry. The apex of the aft-body cone is rounded with a 40-in. radius of curvature. The outer surface of the generic GC is protected with a Thermal Protection System (TPS) to keep the generic GC substructures from overheating. The major dimensions of the GC are listed in table 4.

Table 4. Dimensions of GC.

Height of GC	157.48 in.
Diameter of windward shallow spherical shell	196.85 in.
Outer radius of curvature of windward shallow spherical shell	246.00 in.
Outer radius of curvature of toroidal shoulder	9.00 in.
Leeward cone taper angle	30.25°
Outer radius of rounded apex	40.00 in.

For the shape prediction analysis, a unit width of a section-cut along the vertical plane of symmetry of the GC was considered (fig. 12). Thus, the GC section-cut is then the union of curved and straight beams with a constant depth of $2c = 0.5$ in. Figures 13–15 show the SPAR-generated undeformed and deformed shapes of the GC section-cut under different support conditions. There are $n + 1$ ($n = 32$) equally spaced strain-sensing stations, identified with $i (= 0, 1, 2, 3, \dots, n)$, along the GC section-cut outer surface. In the shape prediction analysis of the GC section-cut, the following three support cases are considered:

- Case 1. Top central point fixed ($i = 0$), and an upward load of $P = 2$ lb is applied at the bottom central point, $i = n$ (fig. 13).
- Case 2. Bottom central point fixed ($i = 0$), and a downward load of $P = 2$ lb is applied at the top central point, $i = n$ (fig. 14).
- Case 3. Two toroidal shoulder points are simply supported (radially movable), and a load of $P = 2$ lb is applied downward and upward respectively at the top and bottom central points. Strain-sensor reference point, $i = 0$, may be assigned at the top or bottom central point (fig. 15).

In order to apply the Displacement Transfer Function, equation (12), for uniform beams, the counting sequence of the strain-sensing stations must be such that the reference strain sensor, $i = 0$, is located at the fixed point, or at a point of symmetry (top or bottom central point) where the slope is zero. Because of a shallow curved beam, the neutral axis is practically located at the half-depth; no inner strain-sensing line is needed for determining the actual location of the neutral axis.

Surface Bending Strain Curve

Figure 16 shows the surface bending strain curve generated by the SPAR program for the GC section-cut. It is important to mention that the strain curves for the support cases 1–3 are identical. In the windward spherical shell region, the bending strain curve is practically a tapering-up straight line, indicating that this

region behaves almost like a straight beam. The strain curve in the leeward cone zone is a tapering-down straight line because of the straight beam region, and then bent down slightly in the rounded apex region. The toroidal region caused an abrupt slope change of the strain curve (fig. 16). The strain data of figure 16 were used as inputs to the Displacement Transfer Function, equation (12), for the shape prediction analysis of the GC section-cut.

Deflection Equation

The Displacement Transfer Function, equation (12), was found to provide very accurate shape predictions in the windward shallow spherical shell region of the GC section-cut (bottom fixed case). However, for the shape prediction of the leeward region (top fixed case), a curvature-correction factor, η_{GC} , is required. Namely,

$$(y_i)_{GC} = \eta_{GC} y_i = \eta_{GC} \left\{ \underbrace{\frac{(\Delta l)^2}{6c} \left[(3i-1)\epsilon_0 + 6 \sum_{j=1}^{i-1} (i-j)\epsilon_j + \epsilon_i \right]}_{\text{Equation (12) with terms } y_0 + (i)\Delta l \tan \theta_0 \text{ removed}} \right\} ; \quad (i=1,2,3, \dots, n) \quad (19)$$

Equation (19) is equation (12) with terms, $y_0 + (i)\Delta l \tan \theta_0$, removed and multiplied by a correction factor, η_{GC} , to account for the complex geometry of the GC section-cut (combination of curved and straight beams). The values of the correction factor, η_{GC} , for different support cases were determined in light of SPAR deflection outputs and are listed in table 5.

Table 5. Geometry correction factor, η_{GC} , for the GC section-cut.

Loading case	η_{GC}
Case 1 (Top fixed)	0.90
Case 2 (Bottom fixed)	1.00 (no correction)
Case 3 (Toroidal shoulders simply supported)	1.00 (no correction)

Deflection Curves

Figure 17 shows the deflection curves for the support case 1 (top fixed). The deflection curve calculated from equation (12) for cantilever straight-beam compares relatively well with the SPAR deflection curve from the apex (fixed point) to the toroidal shoulder. The comparison became very poor in the windward shell region because of a geometrical sharp turn (more than 90°) at the toroidal shoulder, causing a sudden change in the sign of deflections. If the correction factor, $\eta_{CEV} = 0.90$, is introduced (table 5), the corrected deflection curve calculated from equation (19) practically matched the SPAR curve from the fixed apex to the toroidal shoulder, but became very poor in the windward shell region because of a sharp turn at the toroidal shoulder.

For the shape prediction of the windward shell region, it is more advantageous to use the support case 2 (bottom fixed, $i = 0$). Figure 18 shows the deflection curves for the support case 2 (bottom fixed). The deflection curve calculated from equation (12) for the cantilever straight-beam perfectly matched the SPAR deflection curve from the bottom fixed point to the toroidal shoulder, but diverged from the SPAR deflection curve in the leeward region due to the sharp geometrical turn at the toroidal shoulder. If the predicted deflection curve [eq. (12)] in the leeward cone region is shifted upward with a constant shift factor, the

predicted curve will come quite close to the SPAR deflection curve. The support condition and the geometrical sharp turn (more than 90°) at the toroidal shoulder induced this shifting effect.

Figure 19 shows the deflection curves for loading case 3 (radially-free simply supported toroidal shoulder points). For the case 3 supports, the SPAR deflection curve exhibits a slight discontinuity at the toroidal shoulder, ($i = 12$), because of a sharp arc. The two deflection curves calculated from the cantilever straight-beam deflection equation (12) for the different strain-sensing station counting sequences (that is, $i = 0$ on top or on bottom) have practically identical geometrical shapes as the SPAR deflection curve, but with different vertical shifting. If the predicted deflection curves [eq. (12)] are properly shifted upward with a constant shift factor for each predicted deflection curve, each predicted curve will practically match the SPAR deflection curve, indicating that equation (12) can provide fairly accurate GC shape prediction.

DISCUSSION

For the present shape analysis of non-symmetrically loaded curved beams, the load, $P = 2$ lb, was used. For any load, P , other than $P = 2$ lb; the amplitudes, $[\eta$ and $\{\eta_1, \eta_2\}]$, of the sine correction functions must be adjusted in proportion to the new load ratio, $(P \text{ lb})/(2 \text{ lb})$ (for linear elasticity). Also, the present loading point of P is at the three-quarter point from left support. For other loading point cases, the amplitudes, $[\eta$ and $\{\eta_1, \eta_2\}]$, and the functional forms of the sine correction functions could be different and must be determined with the aid of finite-element analyses. The amplitudes, $[\eta$ and $\{\eta_1, \eta_2\}]$, are similar to the load calibration factors or strain-gage factors. If the exact curved-beam Displacement Transfer Functions can be developed, $[\eta$ and $\{\eta_1, \eta_2\}]$ calibrations can be eliminated.

For the shape predictions of cylindrical structures such as aircraft fuselages or booster rockets, subjected to unknown or moving load conditions, one can use multiple strain-sensing lines oriented in the axial directions, instead of in the circumferential direction to avoid curvature-induced errors and $[\eta$ and $\{\eta_1, \eta_2\}]$ calibrations. Using multiple axial strain-sensing lines, the overall deformed shape of the cylindrical structures could be calculated using the straight-beam Displacement Transfer Functions.

For the free-flight structure like GC, there is no stationary reference point. The deflections are in relation to a chosen reference moving point. By choosing the reference point in the toroidal region (case 3), the calculated deformed shape exhibited the most accurate shape among the three cases analyzed. The current analysis of case 3 indicates that by breaking up the strain-sensing line into two parts; one strain-sensing line for the windward shallow curved region, and the other strain-sensing line for leeward region; and choosing the reference point, ($i = 0$), at the toroidal shoulder to count the strain-sensing stations separately in two opposite directions; one could also obtain good shape predictions using equation (12).

CONCLUDING REMARKS

The Displacement Transfer Function previously formulated for the uniform straight beam was applied to shape predictions of non-symmetrically loaded curved beams with varying curvatures. The surface bending strain data needed for input to the Displacement Transfer Function for shape predictions were analytically generated from the finite-element analysis. The shape prediction errors from using the straight-beam Displacement Transfer Function for the curved beams were examined in light of the finite-element-generated deflection curves. The functional forms for the curvature-effect correction terms were established through single-point or dual-point collocations, and were incorporated into the straight-beam Displacement Transfer Function to establish the curved-beam Displacement Transfer Function for shape predictions of non-symmetrically loaded two-end supported curved beams. The straight-beam Displacement Transfer Function

was also used for the shape predictions of a GC outer sandwich shell that has a section-cut with a union of straight and curved beams. The key results of the present shape prediction analysis are itemized below.

1. For non-symmetrically loaded curved beams, the deformed shapes are similar to one-cycle sine waves.
2. Without curvature-effect corrections, the Displacement Transfer Function for the uniform straight beam, provides quite accurate (1.9% error) shape predictions of curved beams (clamped and simply supported) with curved-beam angles up to 45° .
3. For the clamped curved beam cases, two sine-correction functions (with identical amplitude) are required for the left-hand and right-hand regions of the loading point [eq. (16a–b)].
4. For the simply supported curved beam cases, one sine-correction function is required (with different amplitudes) for the left-hand and right-hand regions of the loading point [eq. (18a–b)].
5. For the generic GC complex wall geometry (combination of straight and curved beams), the straight-beam Displacement Transfer Function provides accurate shape predictions in partial regions.
 - a. For the GC apex-fixed case, a 0.9 correction factor was needed for the straight-beam Displacement Transfer Function to give accurate shape predictions in the GC leeward region (combination of straight and curved beams).
 - b. For the GC bottom-fixed case, the straight-beam Displacement Transfer Function (without correction) gives excellent shape predictions in the GC windward spherical region.
 - c. Using the reference point at the GC toroidal shoulder, the straight-beam Displacement Transfer Function gives fairly accurate deformed shape without any correction.

FIGURES

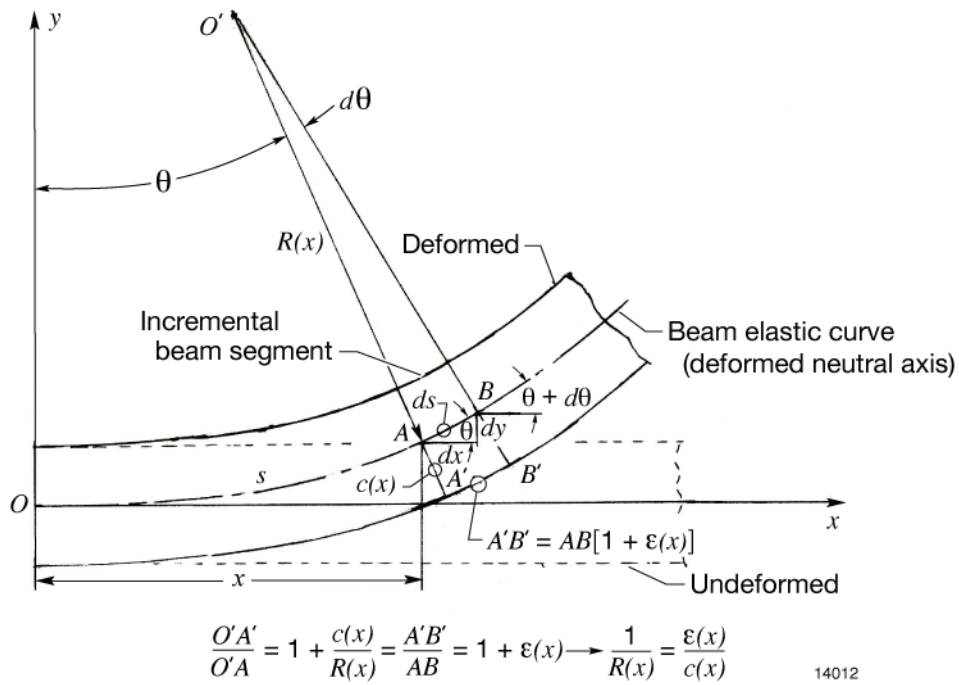


Figure 1. Small segment of the deformed nonuniform embedded beam for relating local radius of curvature, $R(x)$, to associated surface bending strain, $\epsilon(x)$.

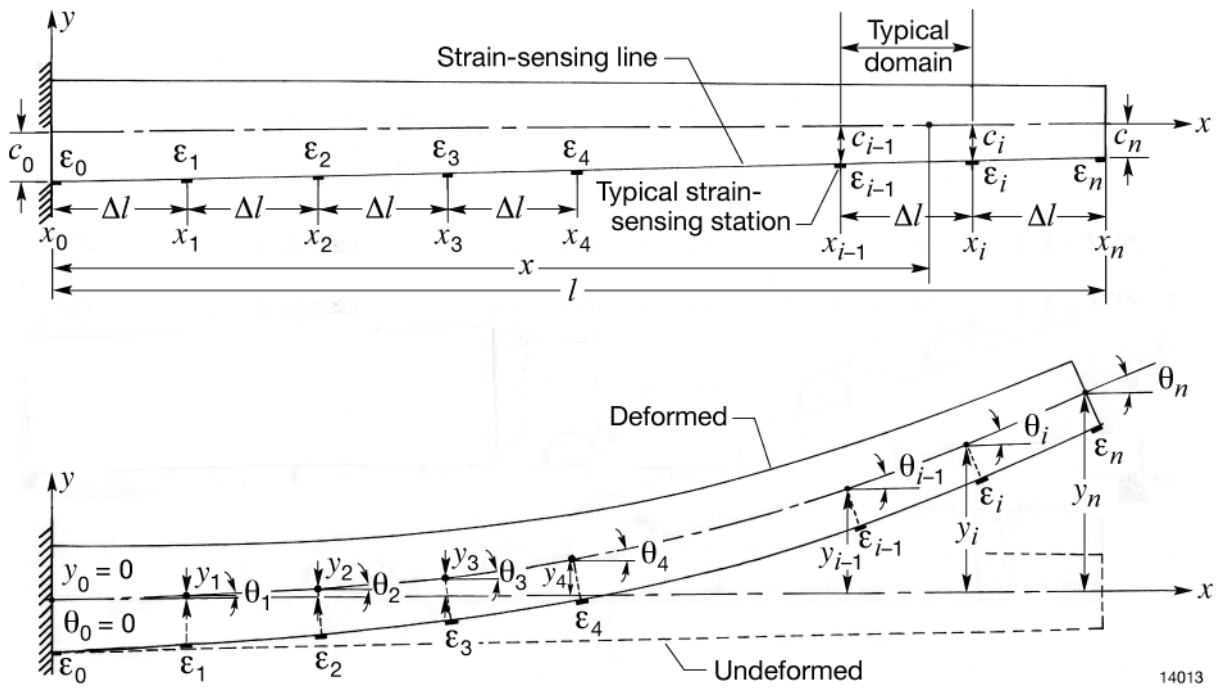


Figure 2. Embedded beam (depth-wise cross section of structure) along the bottom strain-sensing line with evenly distributed strain-sensing stations.

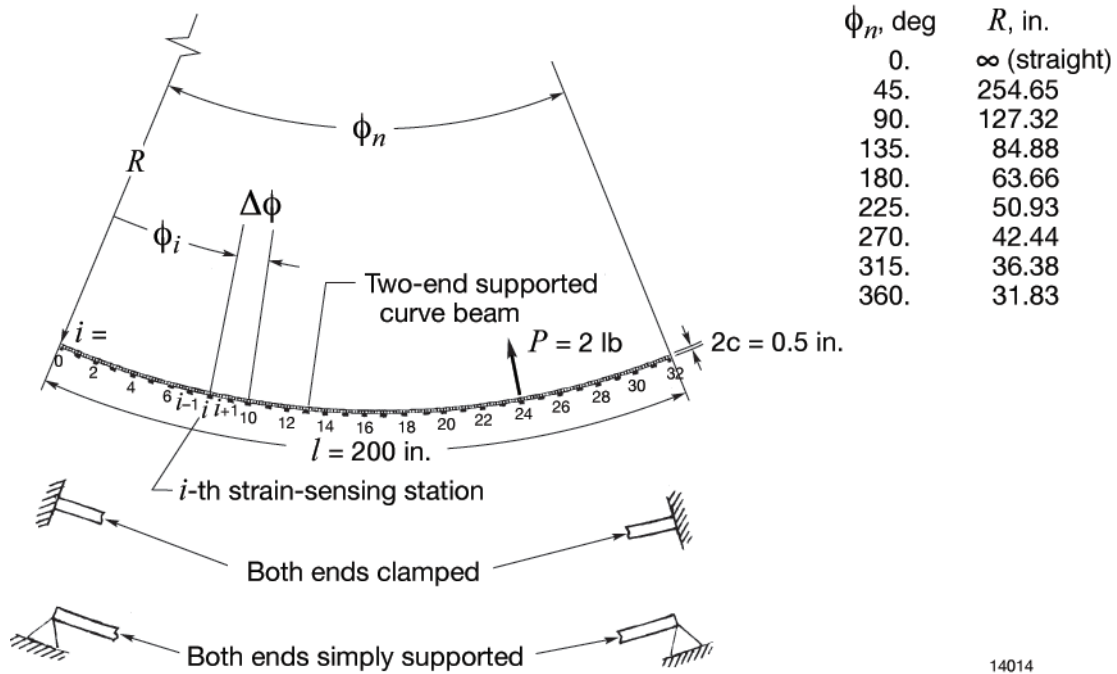
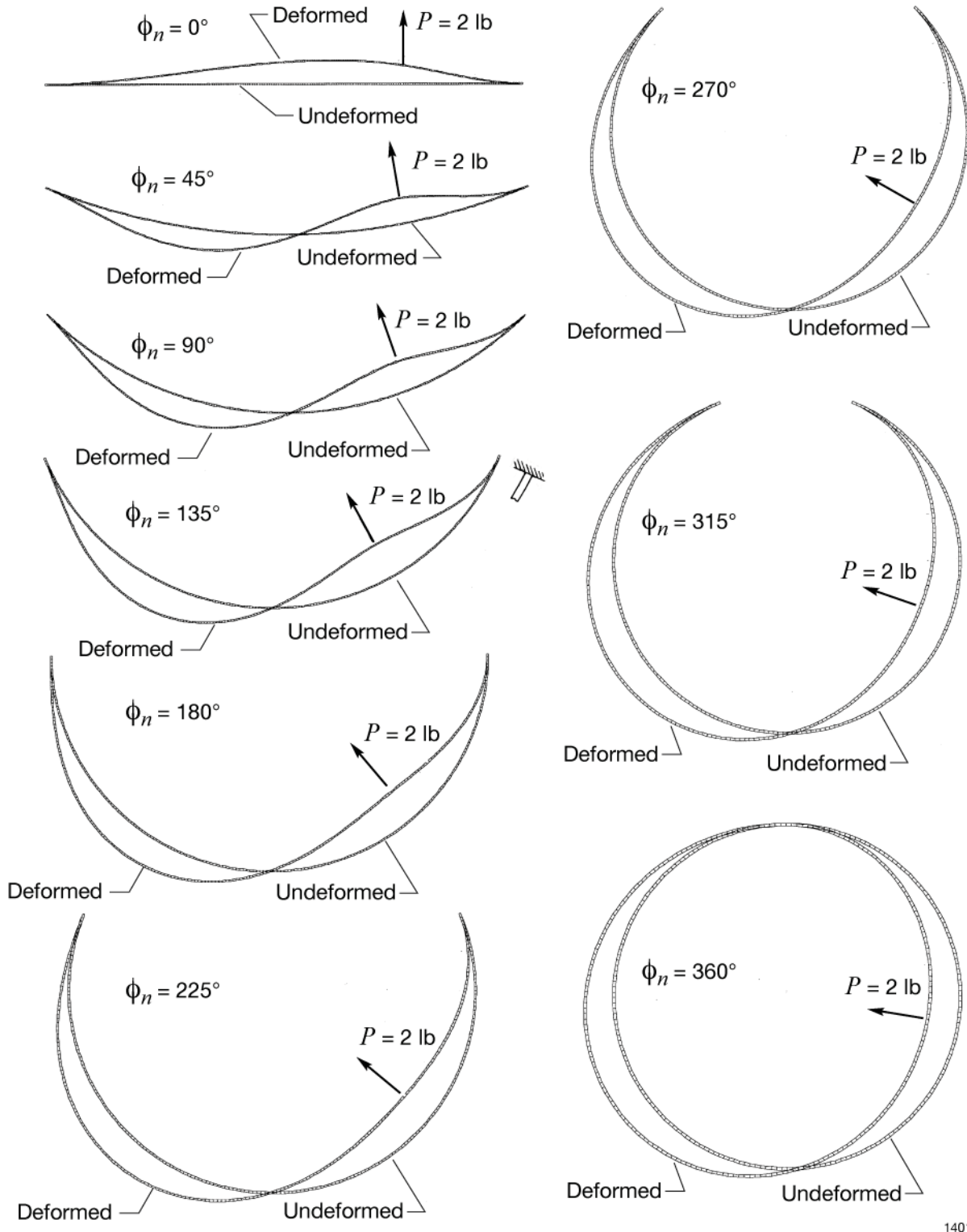


Figure 3. Two-end supported curved beam with $n = 32$ strain-sensing stations on outer surface, subjected to inward radial load of $P = 2$ lb at the three-quarter point strain-sensing station, $i = 24$.



14015

Figure 4. SPAR generated deformed shapes of different clamped curved beams; $P = 2 \text{ lb}$ at the three-quarter point strain-sensing station, $i = 24$.

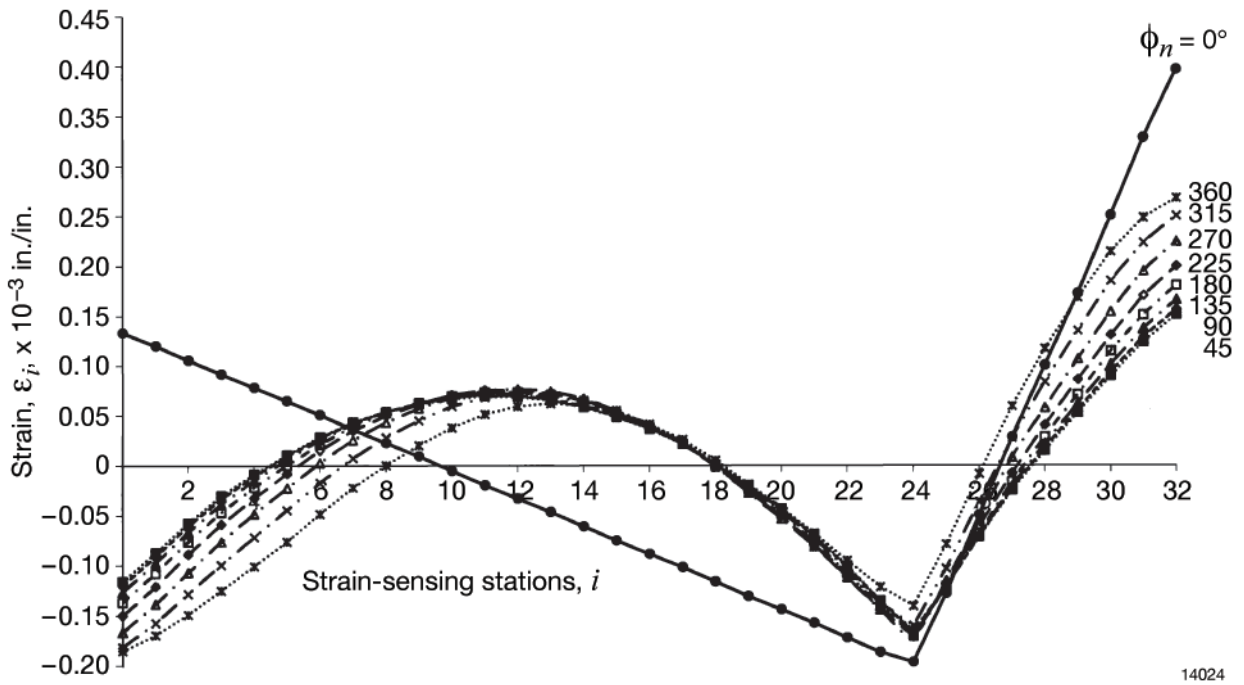


Figure 5. Spar generated surface strains for clamped curved beams with different curvatures; $P = 2$ lb at three quarter point strain-sensing station $i = 24$.

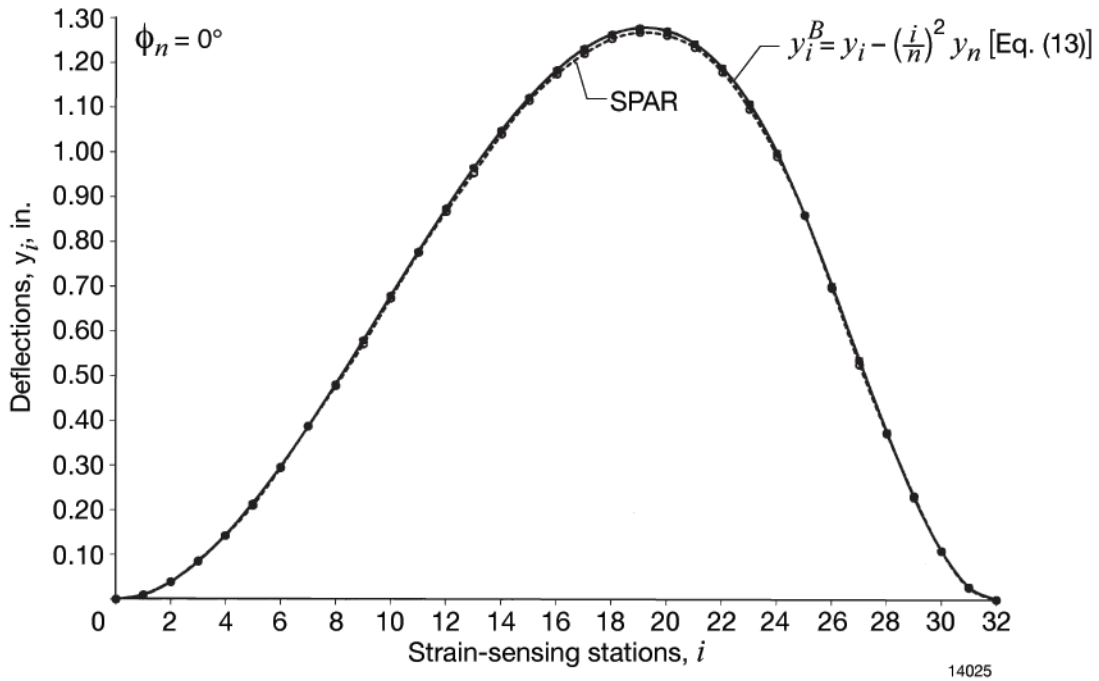
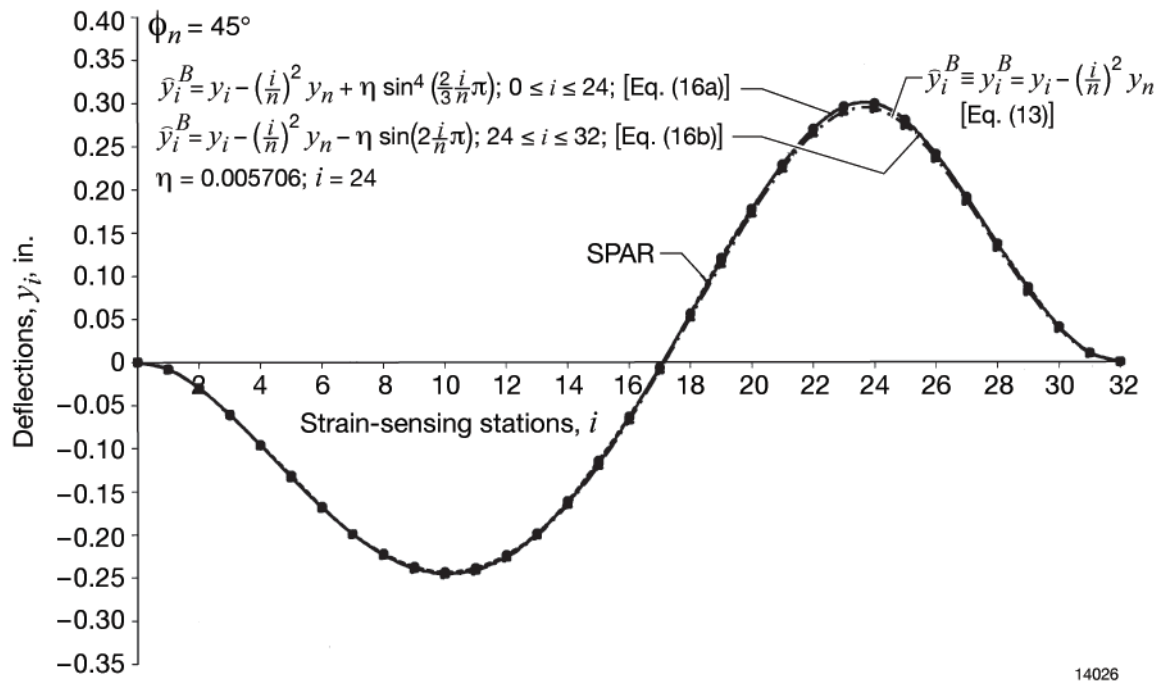


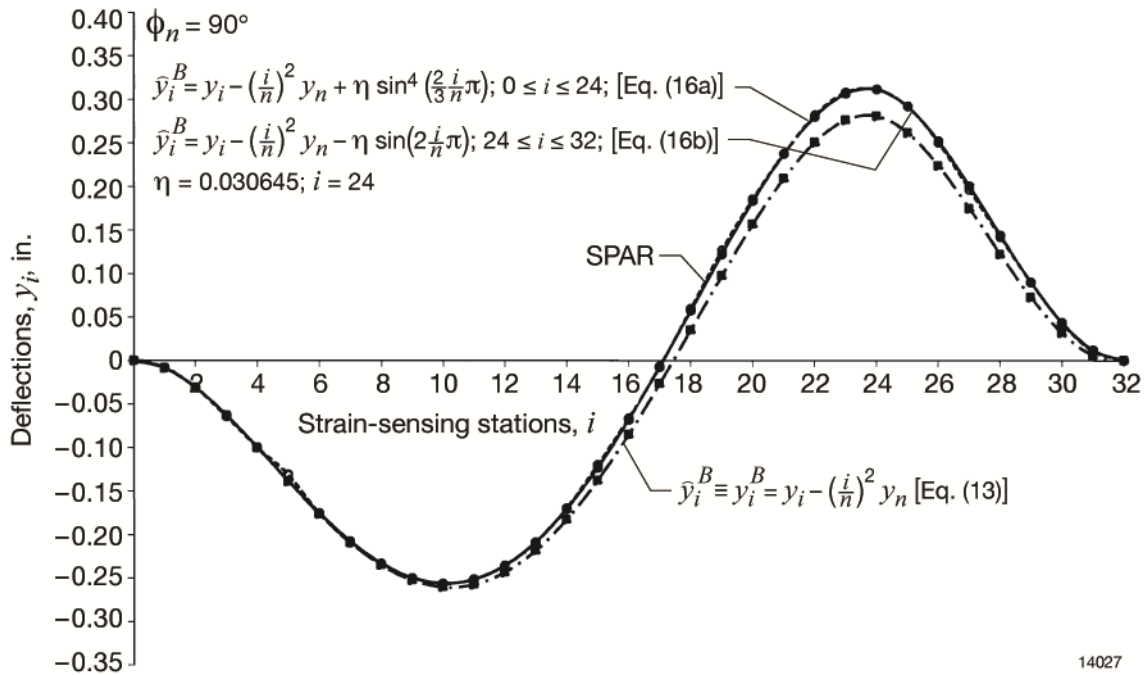
Figure 6(a). $\phi_n = 0^\circ$

Figure 6. Comparison of calculated and SPAR-generated deflection curves for clamped curved beams with different curvatures; $P=2$ lb at the three-quarter point strain-sensing station, $i = 24$.



14026

Figure 6(b). $\phi_n = 45^\circ$



14027

Figure 6(c). $\phi_n = 90^\circ$

Figure 6. Continued.

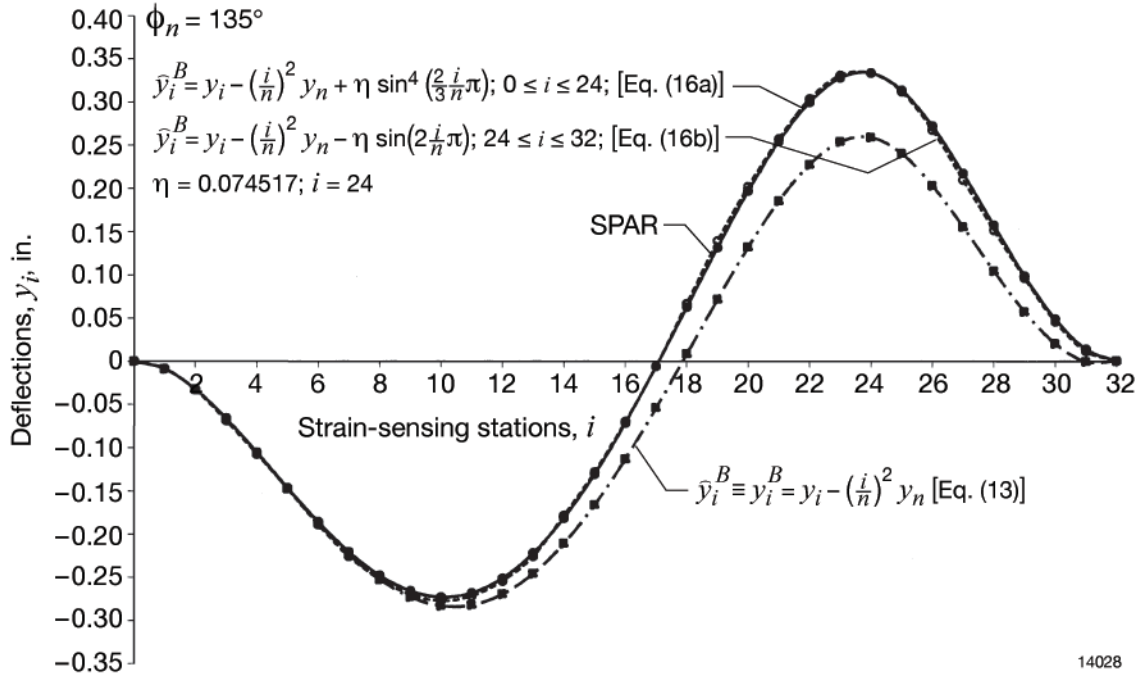


Figure 6(d). $\phi_n = 135^\circ$

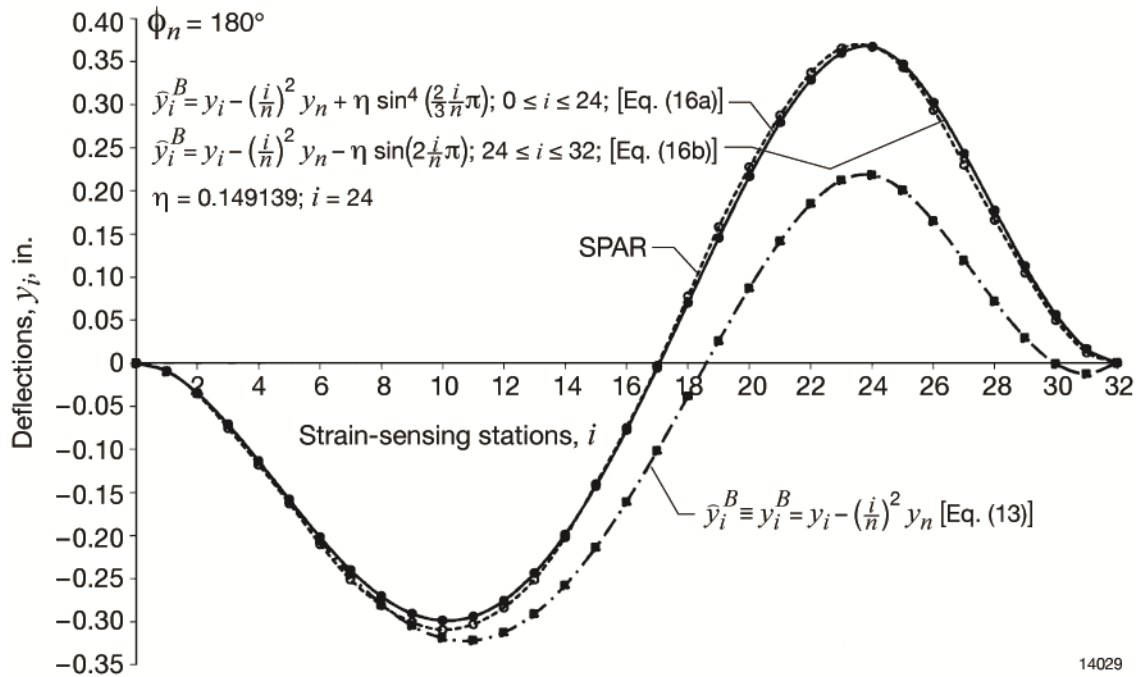


Figure 6(e). $\phi_n = 180^\circ$

Figure 6. Continued.

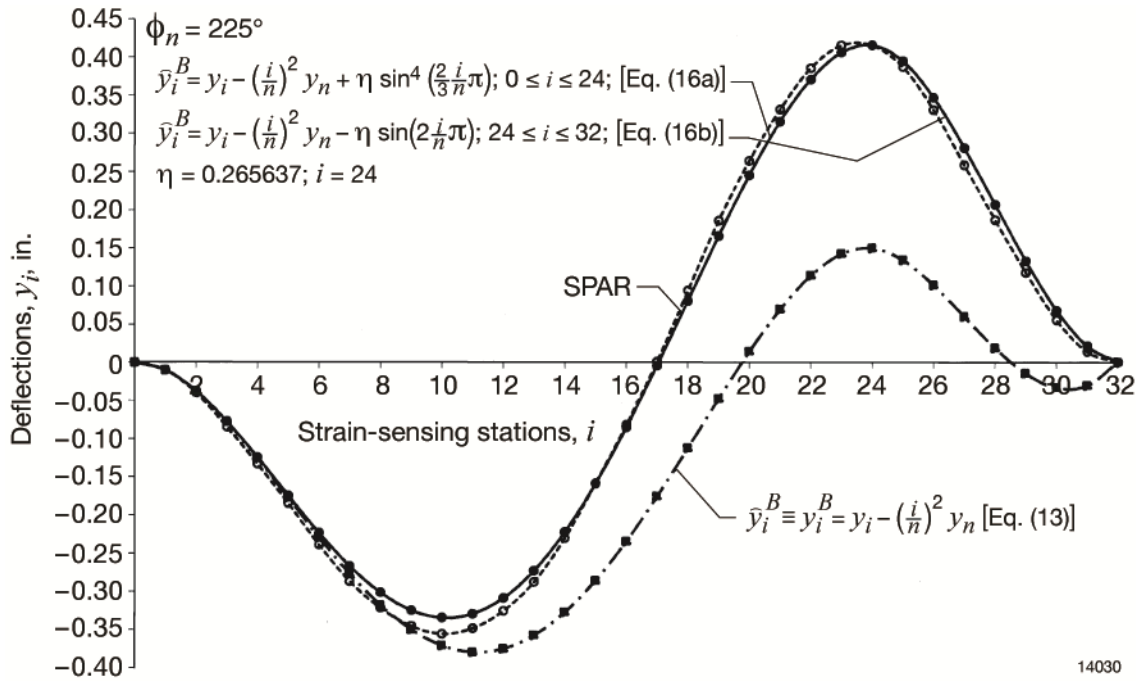


Figure 6(f). $\phi_n = 225^\circ$

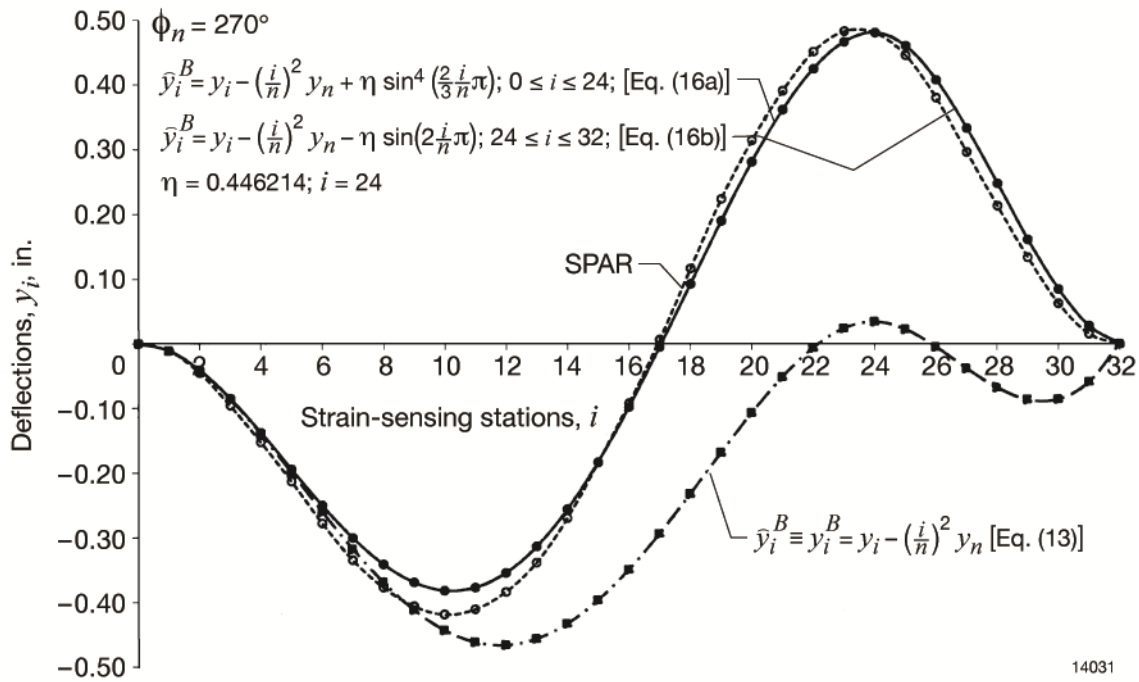


Figure 6(g). $\phi_n = 270^\circ$

Figure 6. Continued.

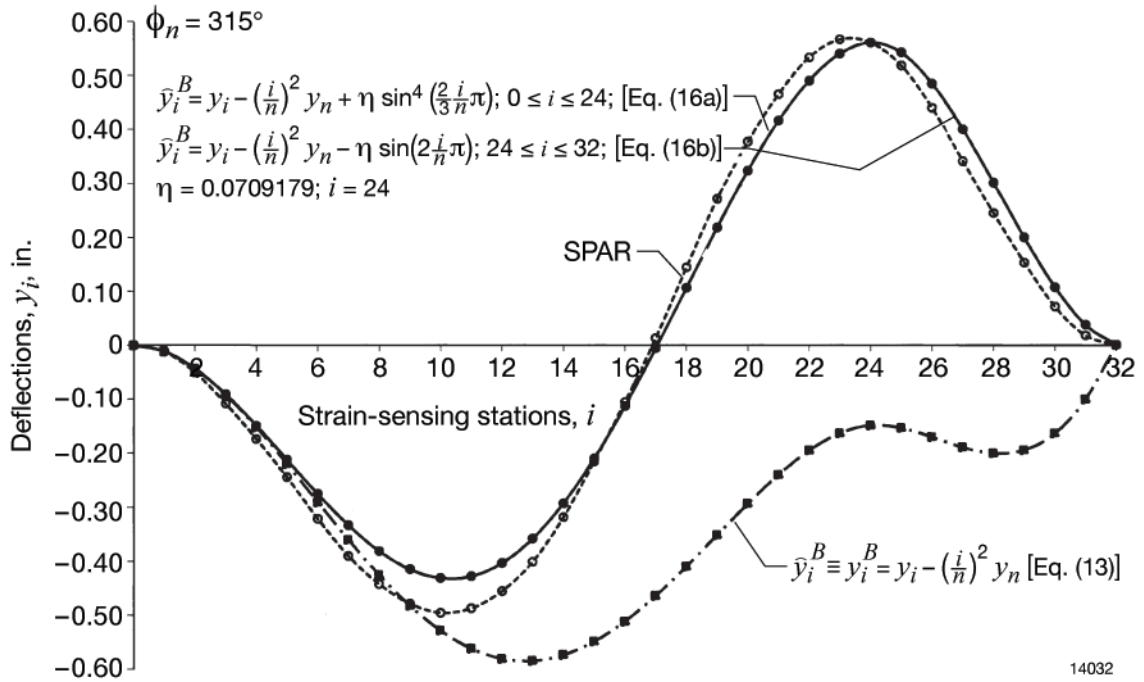


Figure 6(h). $\phi_n = 315^\circ$

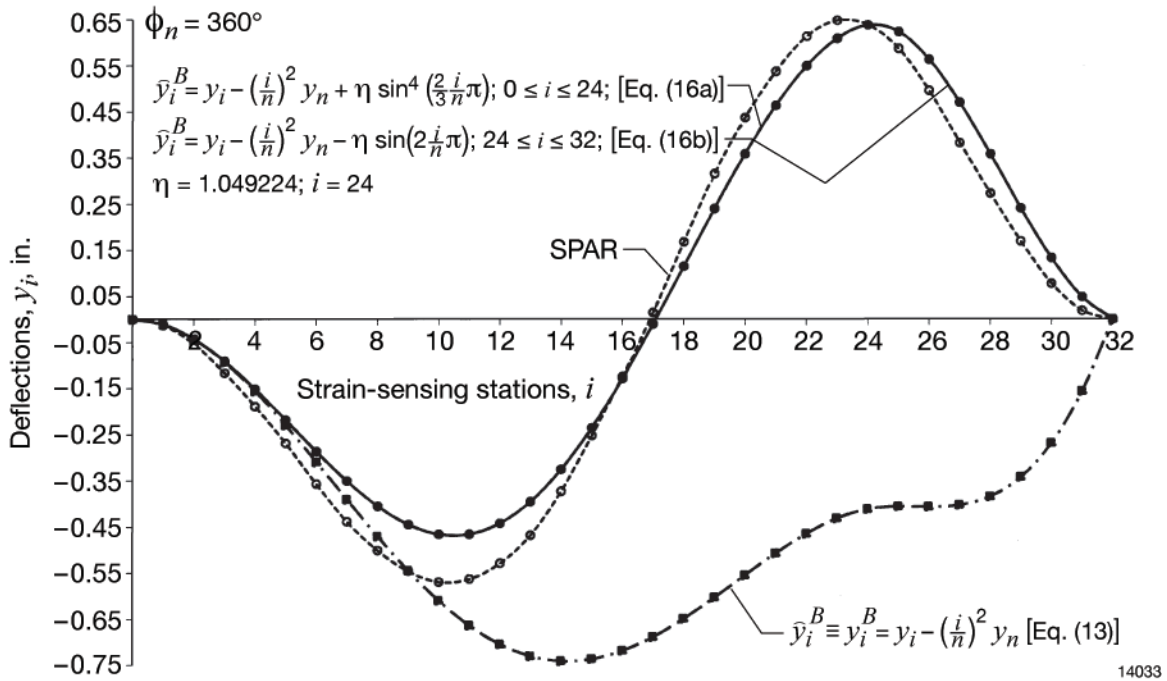


Figure 6(i). $\phi_n = 360^\circ$

Figure 6. Concluded.

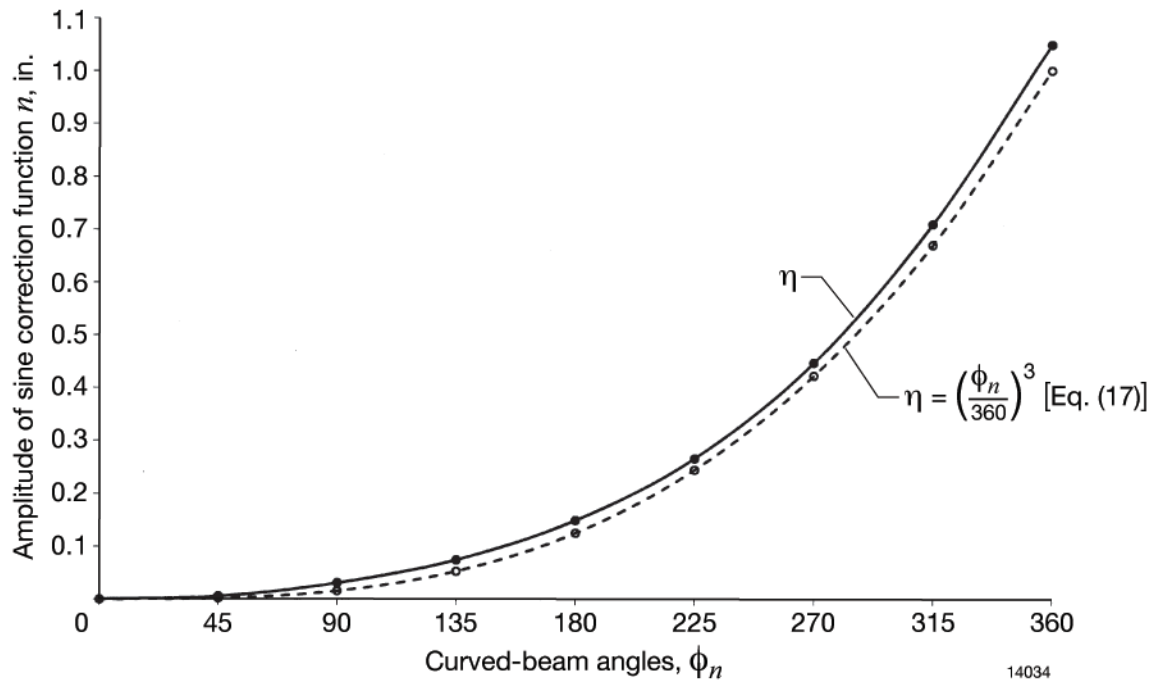
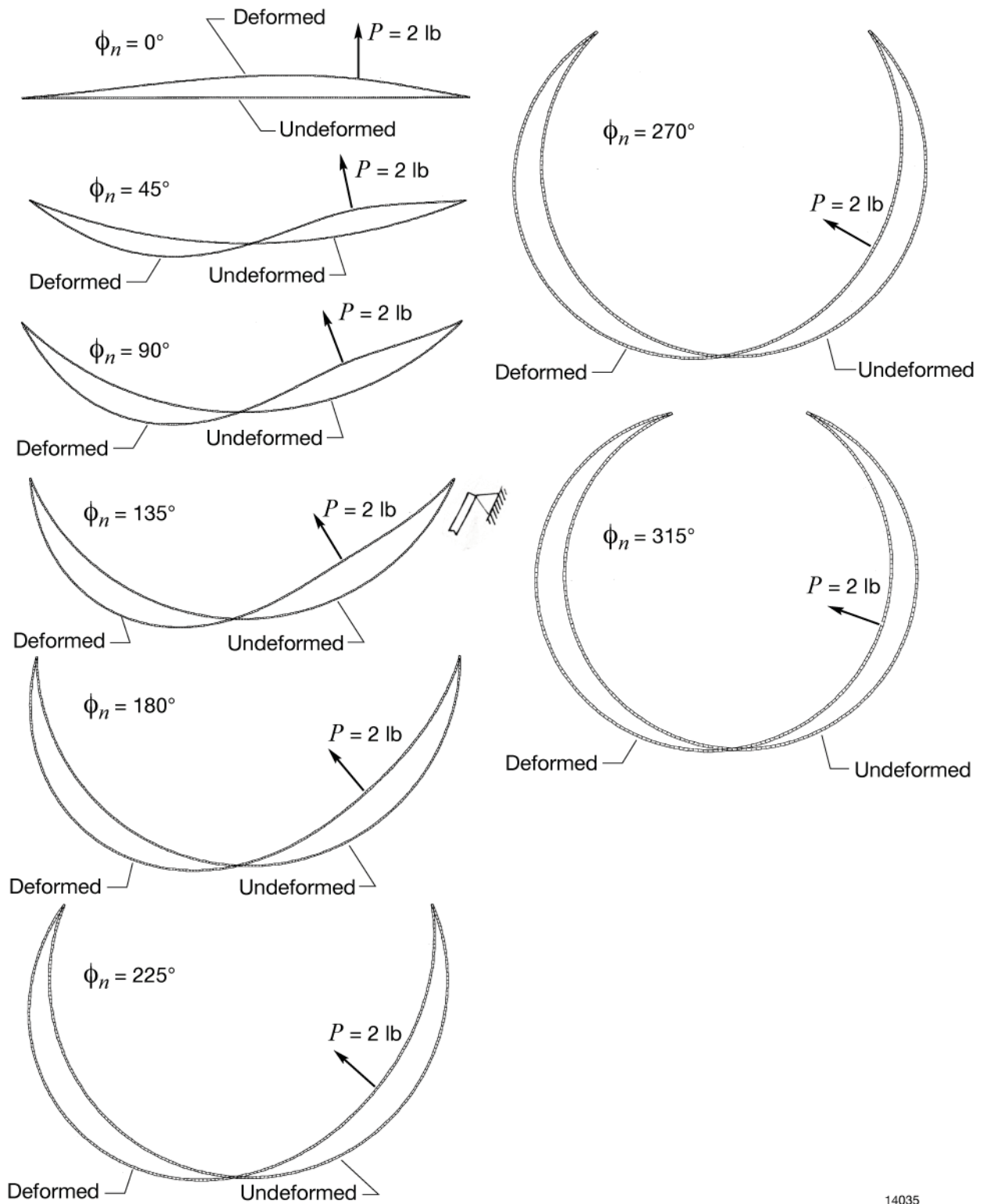


Figure 7. Amplitudes of sine correction functions, η , plotted as functions of the curved beam angle, ϕ_n , for non-symmetrically loaded clamped curved beams.



14035

Figure 8. SPAR generated deformed shapes of different simply supported curved beams; $P = 2 \text{ lb}$ at the three-quarter point strain-sensing station, $i = 24$.

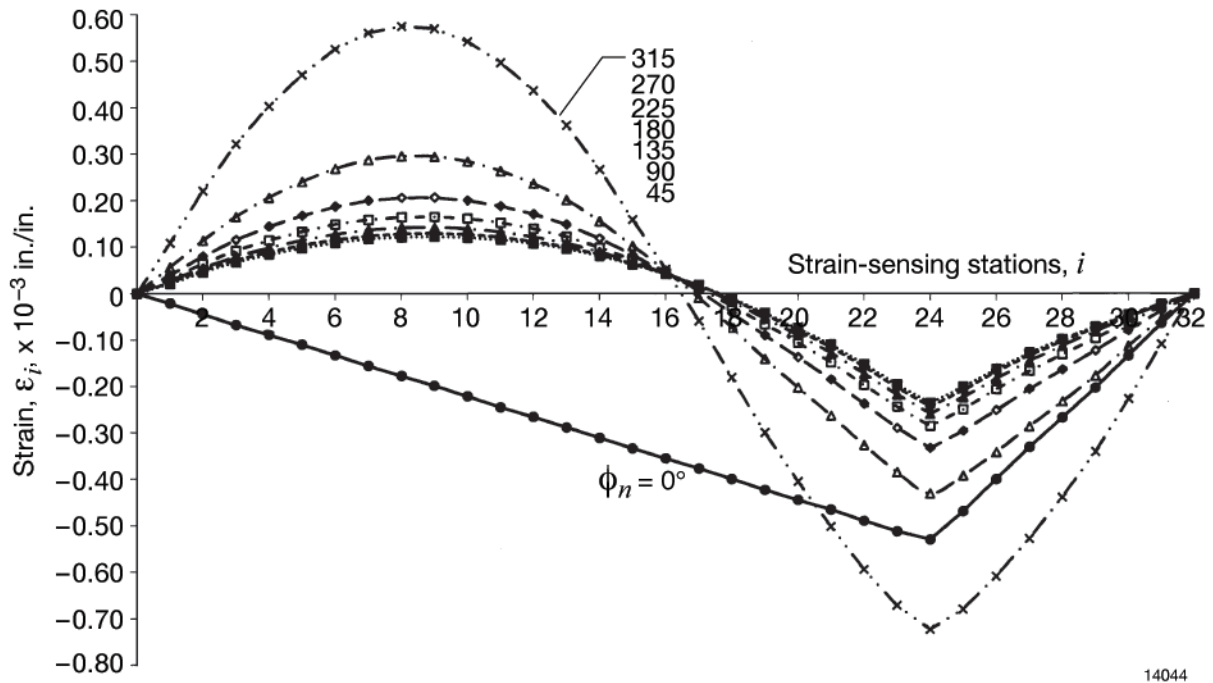


Figure 9. SPAR generated surface bending strains for simply supported curved beams with different curvatures; $P = 2$ lb at the three-quarter point strain-sensing station, $i = 24$.

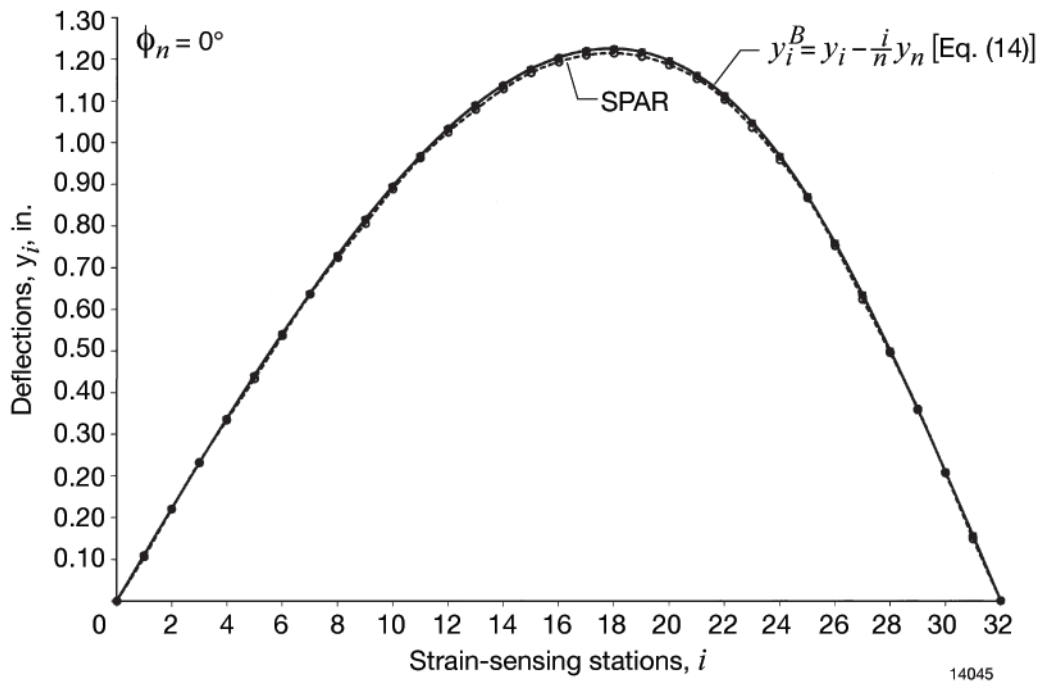


Figure 10(a). $\phi_n = 0^\circ$

Figure 10. Comparison of calculated and SPAR-generated deflection curves for simply supported curved beams with different curvatures; $P = 2$ lb at the three-quarter point strain-sensing station, $i = 24$.

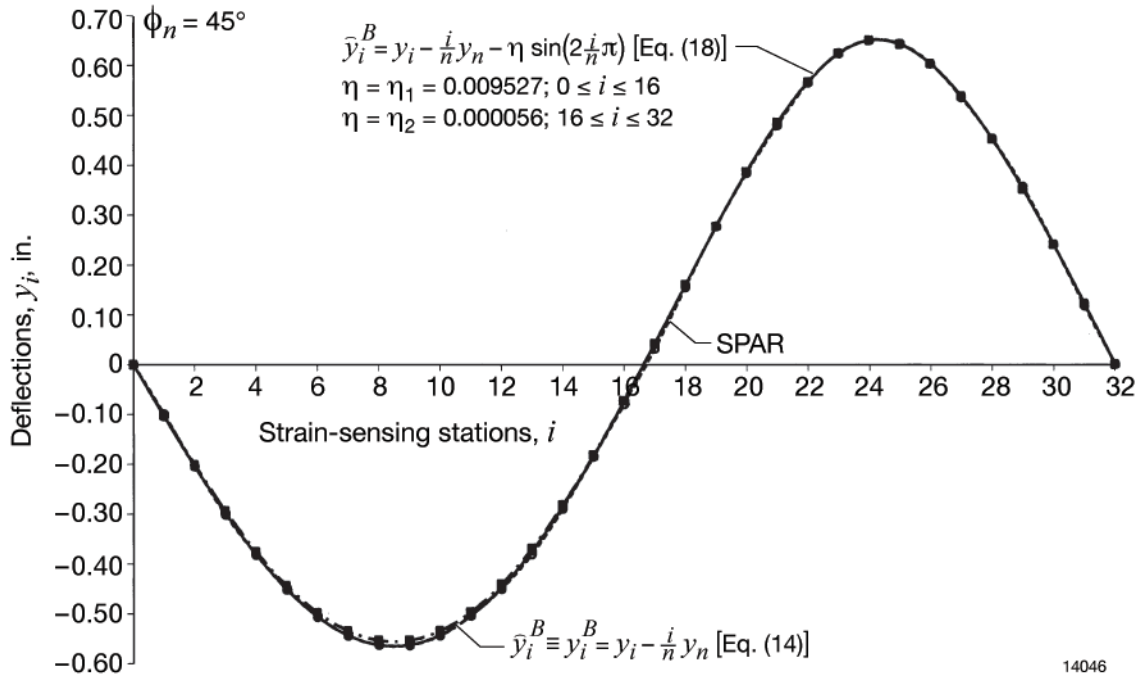


Figure 10(b). $\phi_n = 45^\circ$

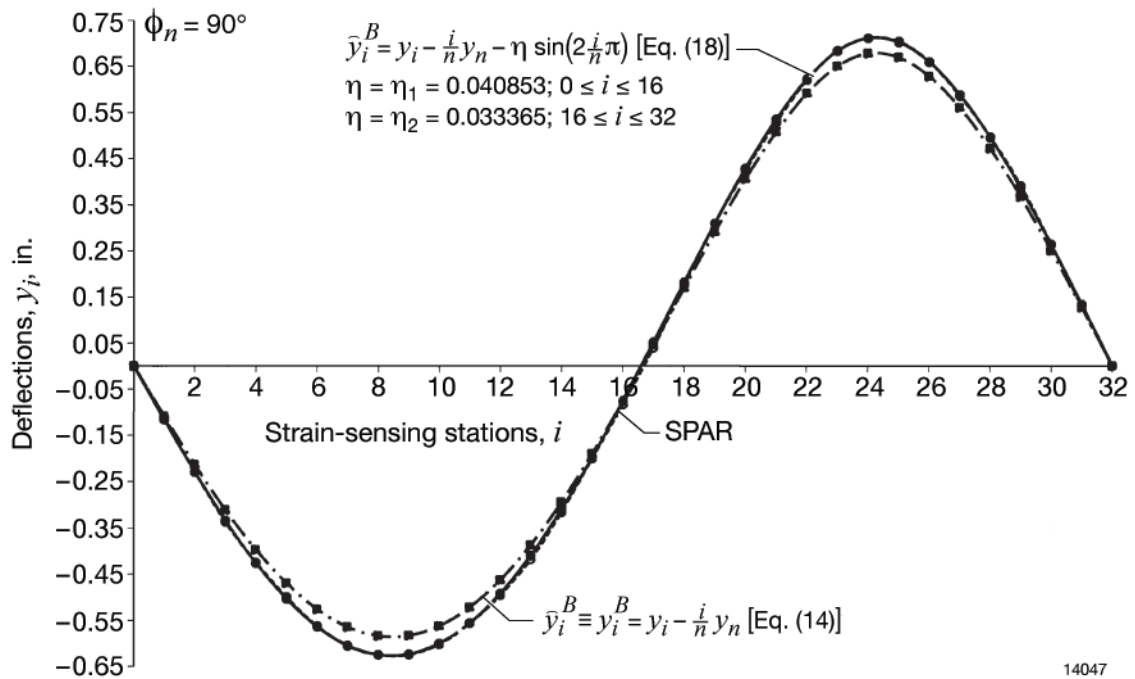


Figure 10(c). $\phi_n = 90^\circ$

Figure 10. Continued.

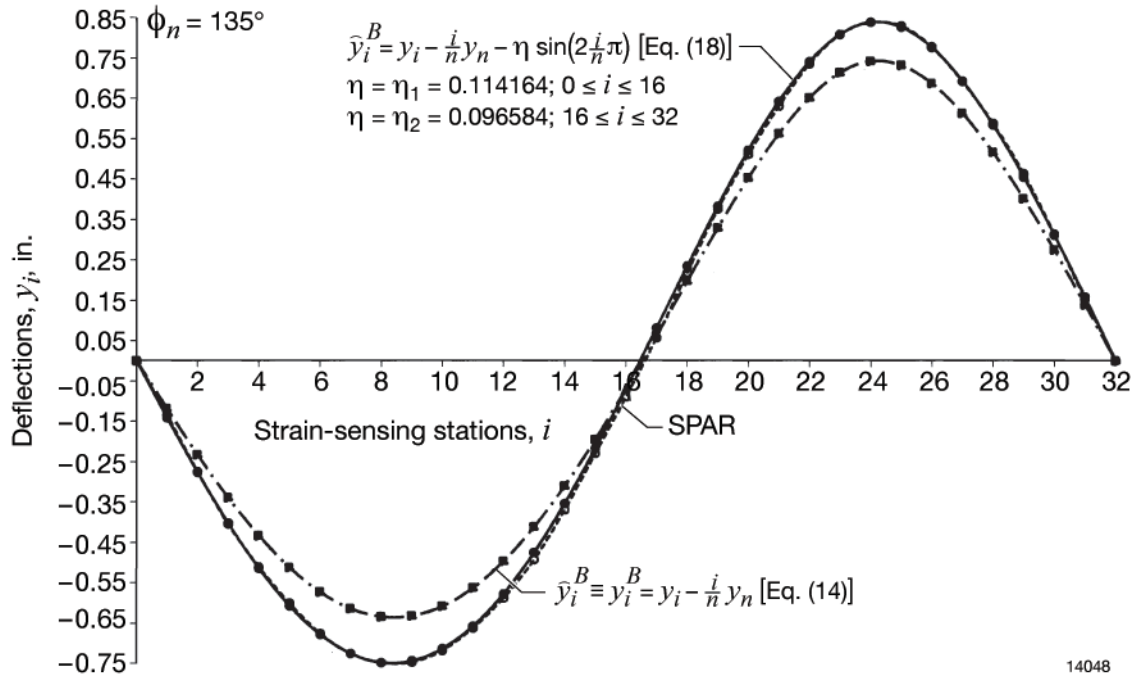


Figure 10(d). $\phi_n = 135^\circ$

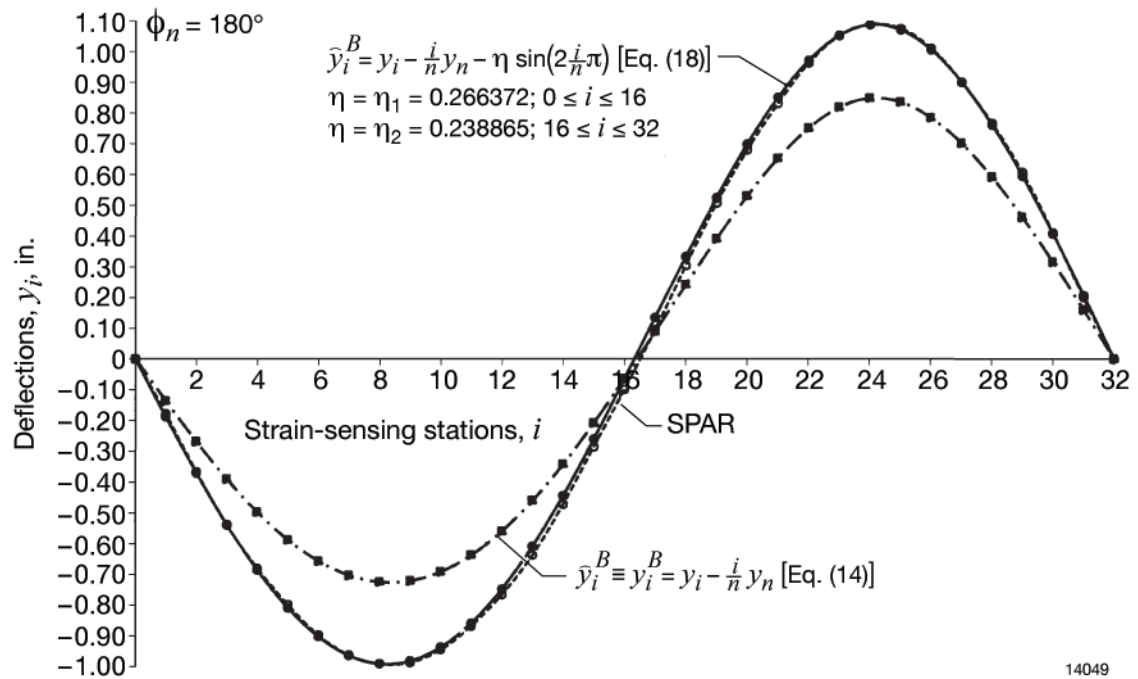


Figure 10(e). $\phi_n = 180^\circ$

Figure 10. Continued.

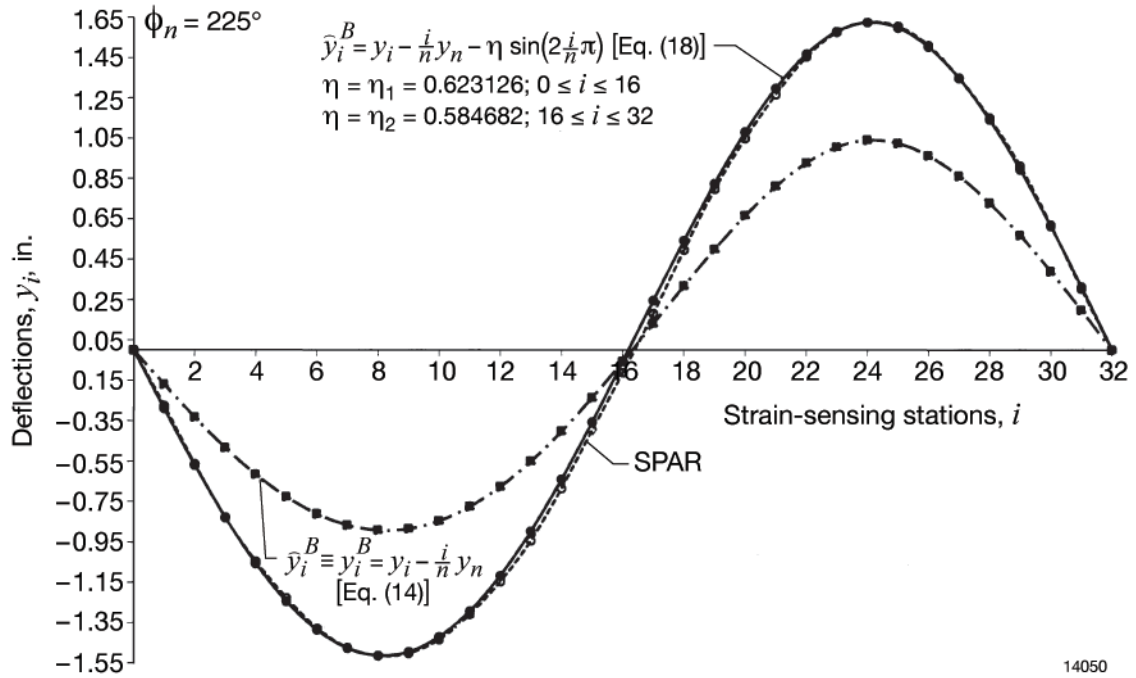


Figure 10(f). $\phi_n = 225^\circ$

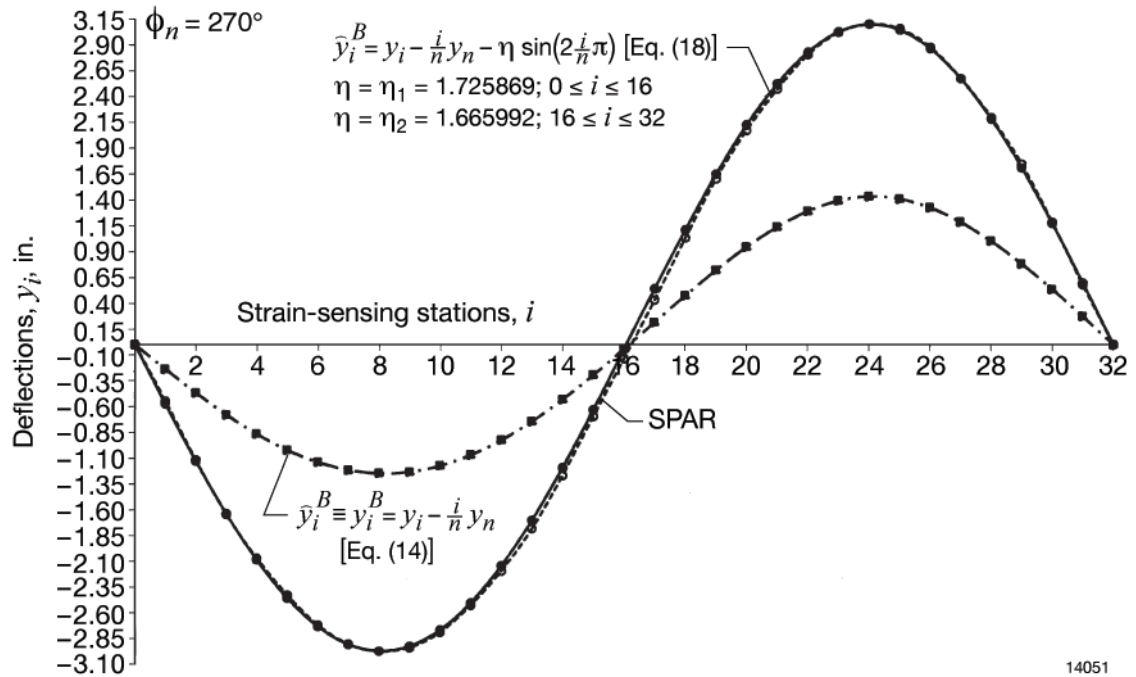


Figure 10(g). $\phi_n = 270^\circ$

Figure 10. Continued.

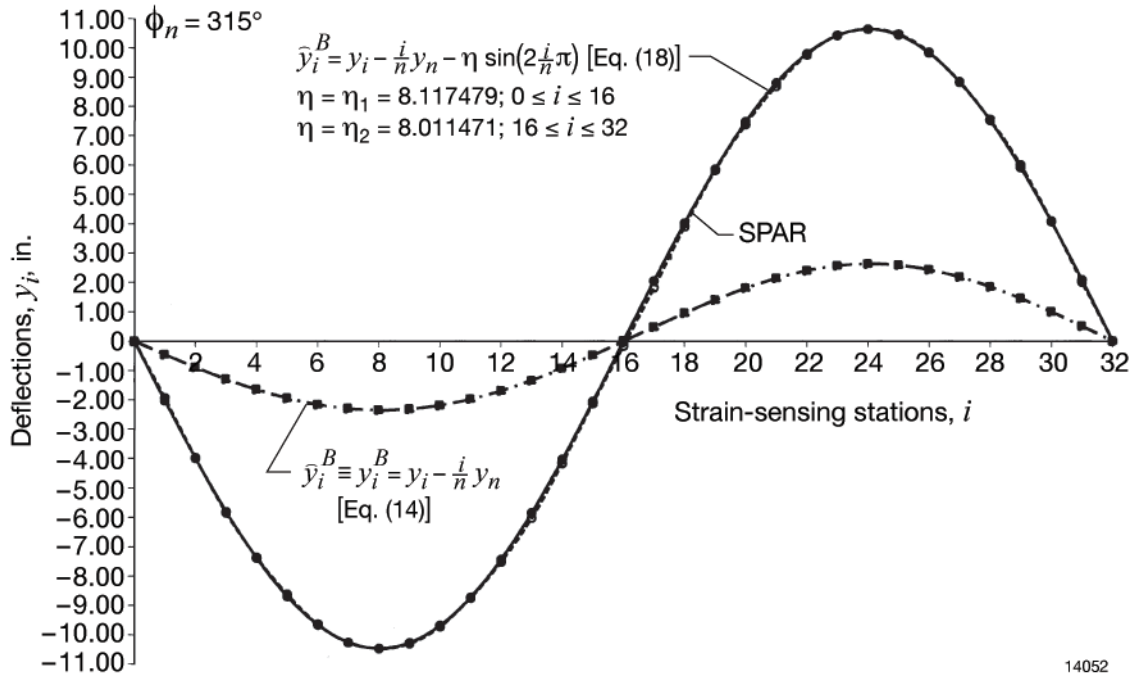


Figure 10(h). $\phi_n = 315^\circ$

Figure 10. Concluded.

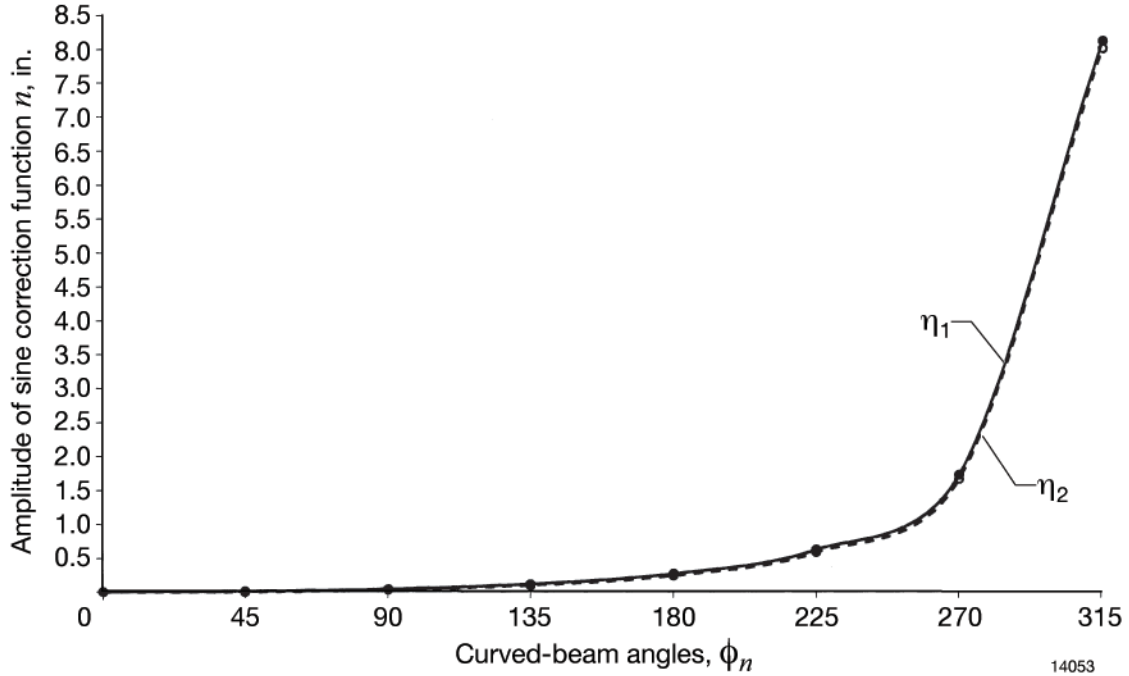


Figure 11. Amplitudes of sine correction functions, $\{\eta_1, \eta_2\}$, plotted as functions of the curved beam angle, ϕ_n , for non-symmetrically loaded simply supported curved beams.

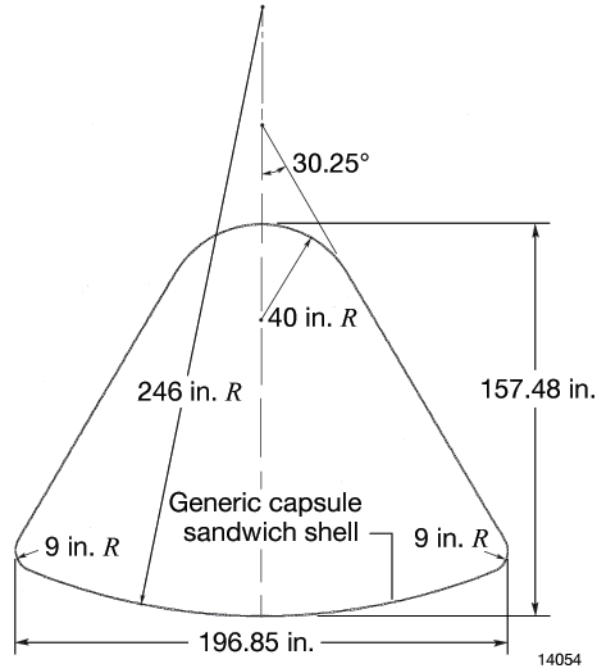


Figure 12. Geometry of the generic capsule walls chosen for shape prediction analysis.

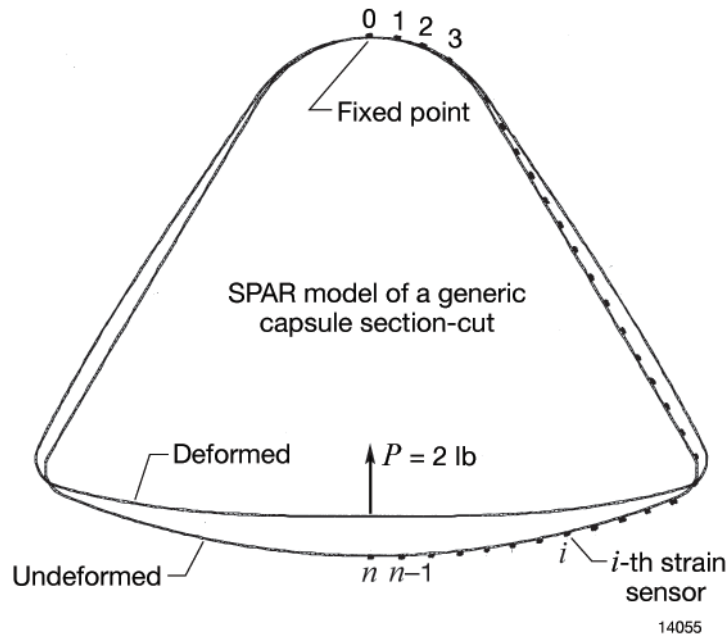


Figure 13. SPAR model for a generic capsule section-cut subjected to an upward load of $P = 2$ lb at an apex with the bottom central point fixed: $n = 32$ strain-sensing stations on a half section-cut.

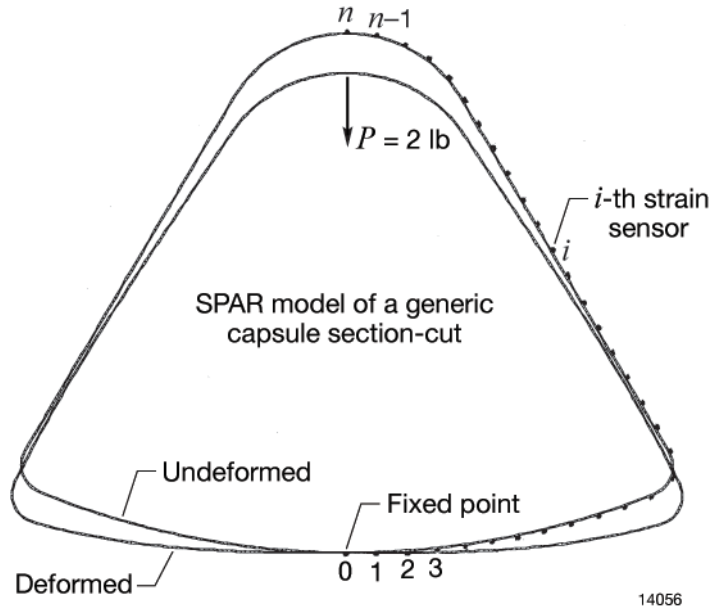


Figure 14. SPAR model for a generic capsule section-cut subjected to a downward load of $P = 2$ lb at an apex with the bottom central point fixed; $n = 32$ strain-sensing stations on a half section-cut.

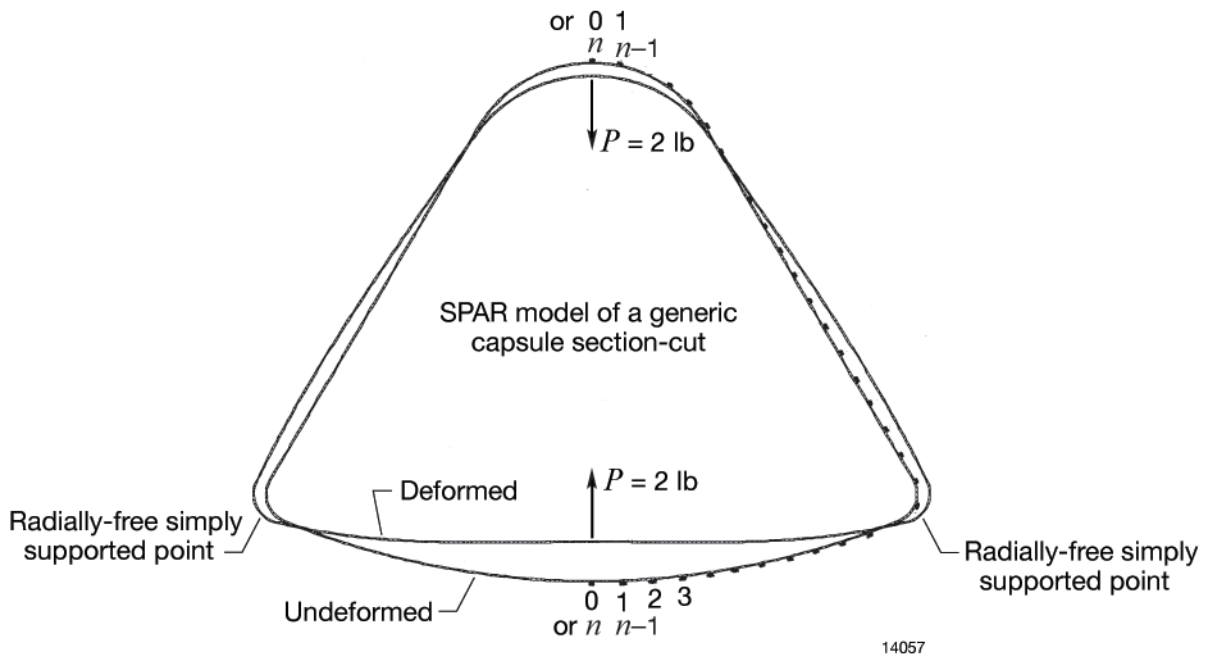


Figure 15. SPAR model for a generic capsule section-cut subjected to an upward and downward load of $P = 2$ lb with toroidal shoulder points simply supported; $n = 32$ strain-sensing stations on a half section-cut.

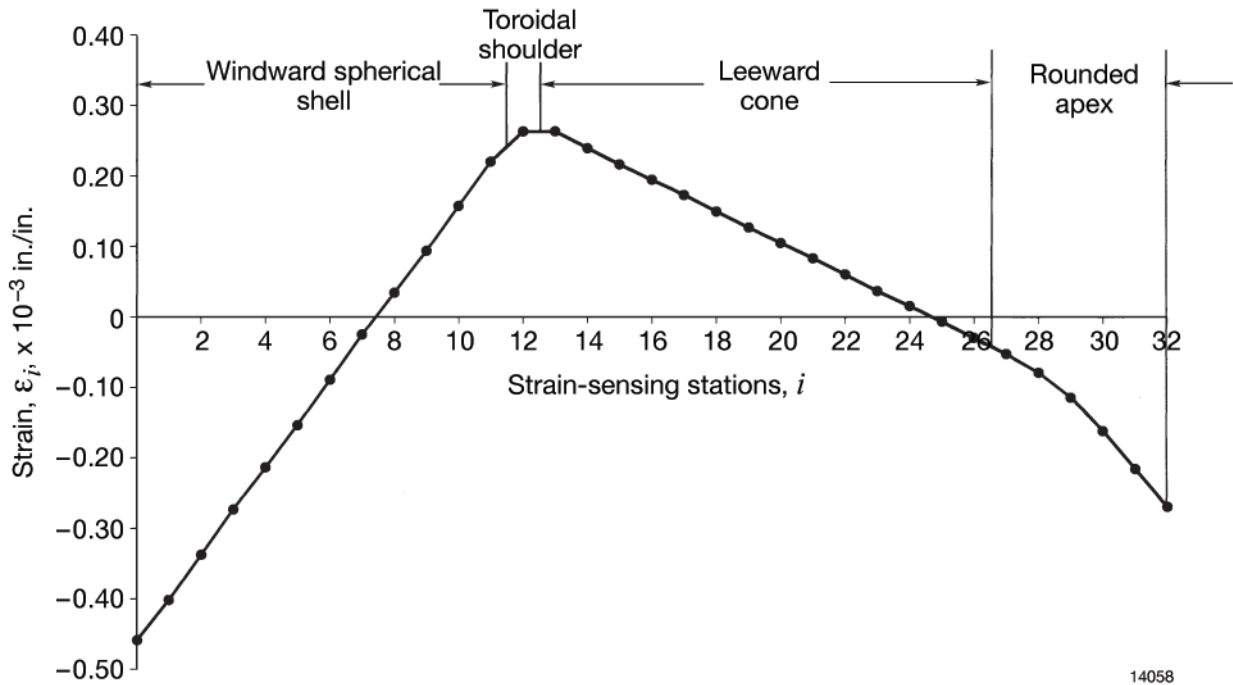


Figure 16. SPAR-generated surface bending strains plotted along a generic capsule wall; identical for three loading cases.

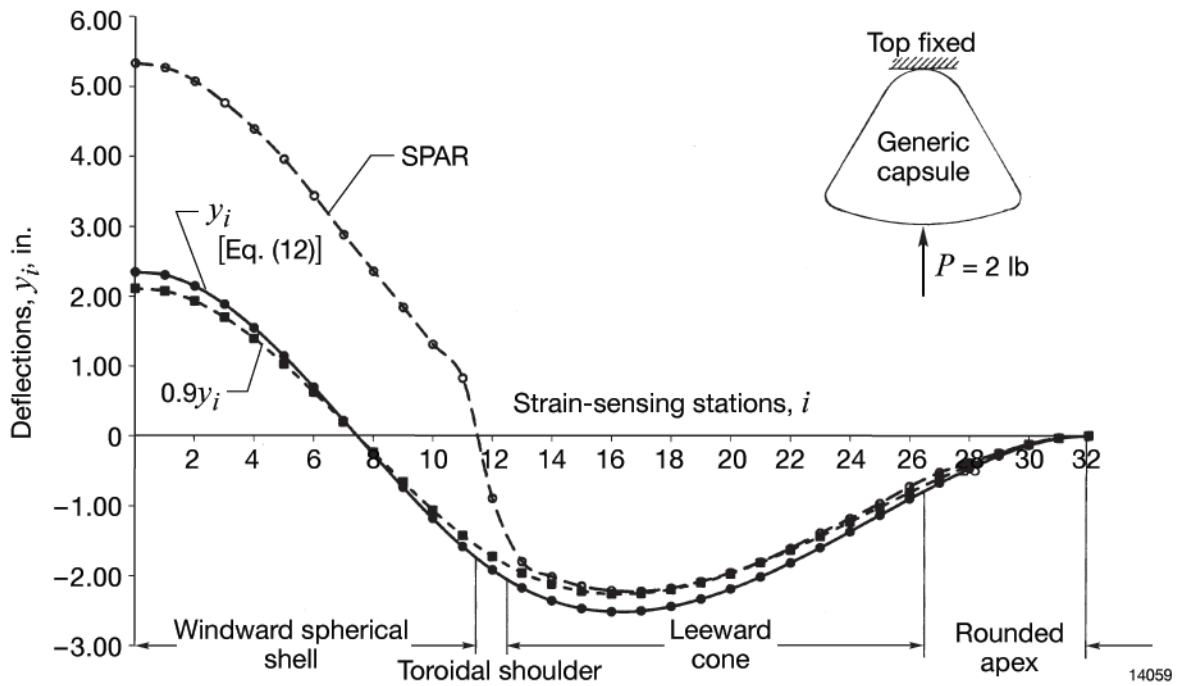


Figure 17. Comparison of predicted and SPAR-generated deflection curves for a generic capsule wall for loading case 1 (top fixed).

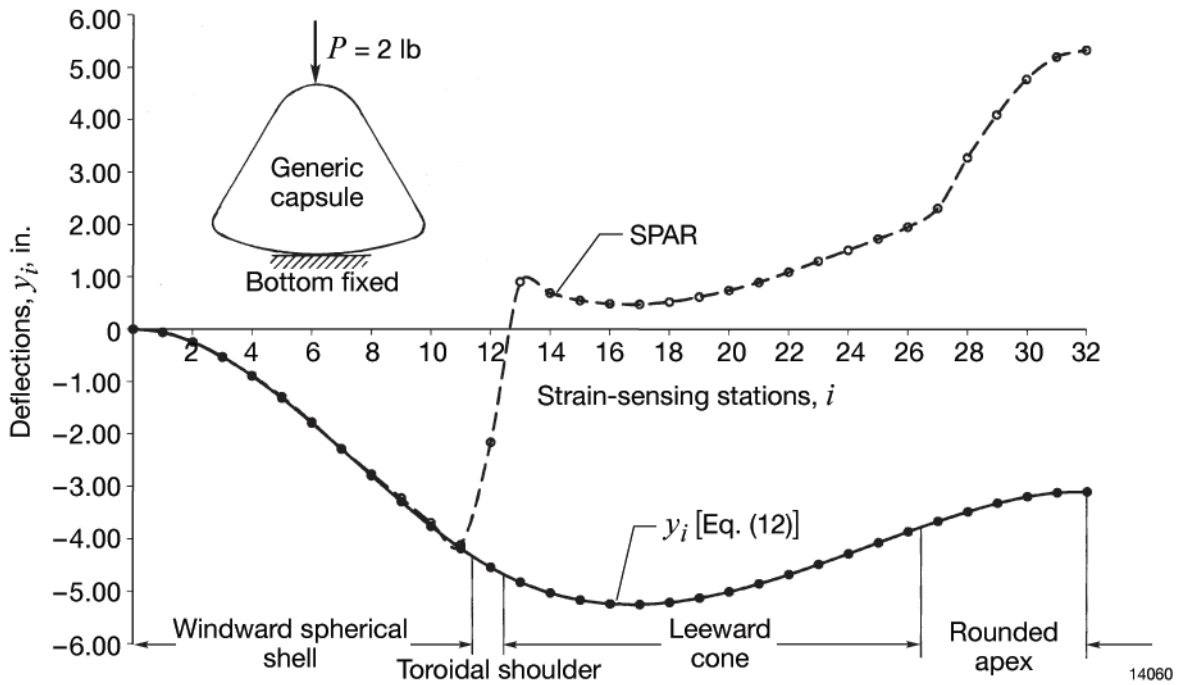


Figure 18. Comparison of predicted and SPAR-generated deflection curves for a generic capsule wall for loading case 2 (bottom fixed).

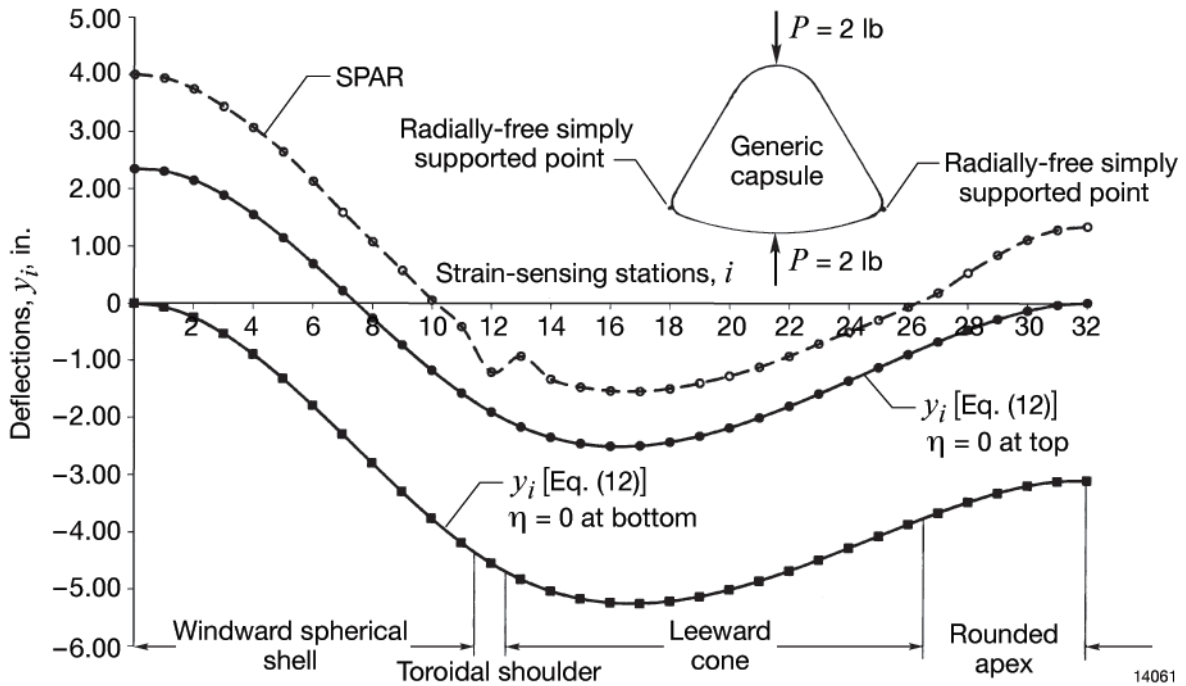


Figure 19. Comparison of predicted and SPAR-generated deflection curves for a generic capsule wall for loading case 3 (toroidal shoulder points radially-free simply supported).

REFERENCES

1. Ko, William L., W. L. Richards, and Van T. Tran, *Displacement Theories for In-Flight Deformed Shape Predictions of Aerospace Structures*, NASA/TP-2007-214612, October 2007.
2. Ko, William L., and Van Tran Fleischer, *Further Development of Ko Displacement Theory for Deformed Shape Predictions of Non-Uniform Aerospace Structures*, NASA/TP-2009-214643, September 2009.
3. Ko, William L., *Collection of Memoranda on Applications of Ko Displacement Theory to Deformed Shape Predictions of Aerospace Structures*, NASA/BR-119, April 2008.
4. Ko, William L., W. L. Richards, and Van Tran Fleischer, *Applications of Ko Displacement Theory to the Deformed Shape Predictions of Doubly Tapered Ikhana Wing*, NASA/TP-2009-214652, November 2009.
5. Ko, William L., and Van Tran Fleischer, *Methods for In-Flight Wing Shape Predictions of Highly Flexible Aerospace Structures: Formulation of Ko Displacement Theory*, NASA/TP-2010-214656, August 2010.
6. Ko, William L., and Van Tran Fleischer, *First and Second Order Displacement Transfer Functions for Structure Shape Calculations Using Analytically Predicted Surface Strains*, NASA/TP-2012-215976, March 2012.
7. Ko, William L., and Van Tran Fleischer, *Improved Displacement Transfer Functions for Structure Deformed Shape Predictions Using Discretely Distributed Surface Strains*, NASA/TP-2012-216060, November 2012.
8. Ko, William L., and Van Tran Fleischer, *Large-Deformation Displacement Transfer Functions for Shape Predictions of Highly Flexible Slender Aerospace Structures*, NASA/TP-2013-216550, November 2013.
9. Ko, William L., and W. Lance Richards, *Method for Real-Time Structure Shape-Sensing*, U.S. Patent No. 7,520,176, issued April 21, 2009.
10. Richards, W. Lance, and William L. Ko, *Process for Using Surface Strain Measurements to Obtain Operational Loads for Complex Structures*, U.S. Patent No. 7,715,994, issued May 11, 2010.
11. Jutte, Christine, William L. Ko, Craig Stephens, John Bakalyar, Lance Richards, and Allen Parker, *Deformed Shape Calculations of a Full-Scale Wing Using Fiber Optic Strain Data from a Ground Loads Test*, NASA/TP-2011-215975, December 2011.
12. Ko, William L., and Van Tran Fleischer, *Extension of Ko Straight-Beam Displacement Theory to Deformed Shape Predictions of Slender Curved Structures*, NASA/TP-2011-214567, April 2011.
13. Whetstone, W. D., *SPAR Structural Analysis System Reference Manual, System Level 13A, Volume 1, Program Execution*, NASA CR-158970-1, December 1978.
14. Ko, William L. Van T. Tran, and Jeff Bowles, *Lunar Return Reentry Thermal Analysis of a Generic Crew Exploration Vehicle Wall Structures*, NASA/TM-2007-214627, October 2007.